nature communications

Article

https://doi.org/10.1038/s41467-026-72909-4

Identification and quantification of intracellular N-acetylglucosamine modified glycoRNAs

Received: 24 October 2025

Accepted: 24 April 2026

Published online: 12 May 2026

Check for updates

Yi Ren, Yuexuan Meng, Huipu Liu, Guangming Li, Jiahui Sun, Jun Zhou, Jie Wu, Ying Liu, Lin Ding, Yunlong Chen ✉ & Huangxian Ju ✉

GlycoRNAs are recently discovered glycoconjugates, their different components and distributions are urgently-to-study issues. Here, we design a general paradigm to study glycoRNA from multiple perspectives. Using the metabolic labelling technology and the designed fluorescent DNA probes, the N-acetylglucosamine (GlcNAc) modified Y5 RNA is identified to be mainly in nucleus by fluorescence resonance energy transfer imaging. After it is collected by a target-specific capture procedure, the component of GlcNAc conjugated ribonucleotide can be determined by gel electrophoresis and mass spectrometric analysis. The levels of intracellular GlcNAc modified Y5 RNA in different cell lines are in situ quantified with a GlcNAc-specific in situ hybridization-mediated proximity ligation assay with single-cell and single-molecule resolution. These findings innovate the distribution and quantitation information of glycoRNAs, which greatly promotes the functional research of glycoRNAs.

Glycans are one of the most important biological molecules, which decorate all mammalian cells[1,2]. They play essential roles in various biological events happened on cell surface, such as cell-cell communication, host-pathogen interactions and immune response[3,4], and thus further affect intracellular biological processes, including cell growth, differentiation and embryogenesis[5,6]. Generally, glycans are believed to be attached only on proteins or lipids through the glycosylation processes in the presence of glycosyltransferases and glycosidases[7]. According to the different attaching modes to the proteins, the glycans are mainly divided into N-glycans, O-glycans and glycosaminoglycans, which bind on Asn and Ser/Thr residues of proteins, Ser residues of proteoglycan molecules, respectively[8,9]. Besides, monosaccharide such as N-acetyl-glucosamine (GlcNAc) has been found to be attached on Ser/Thr residues of intracellular proteins[10,11], and glycosylated small noncoding RNAs (sncRNAs) have also been reported[12], which unveiled the mystery of glycoRNAs.

SncRNAs are extensively distributed in various eukaryotic organisms to perform diverse functions[13,14]. Although some canonical sncRNAs, such as small interfering RNAs and microRNAs, have been well studied and characterized[15], both the compositions and functions of the vast majority of non-canonical sncRNAs, including transfer RNA[16], tRNA-derived small RNA, ribosomal RNA[17], Y RNA[18], small nuclear RNA[19], small nucleolar RNA[20], vault RNA and messenger RNA, are unclear. These non-canonical sncRNAs are generally derived from longer RNAs and regulated by genetic and environmental factors, are thus associated with many diseases[21,22]. For example, human Y RNAs that contain characteristic stem-loop secondary structures with high sequence conservations[23] are related with lupus, Sjögren's syndrome and lung cancer[18,24], and the ability to visualize and quantitatively profile Y RNA at the single-cell resolution[25] is crucial for uncovering the molecular mechanisms underlying Y RNA-associated pathologies and for developing targeted therapeutic strategies for these diseases. Since the discovery of N-glycosylated RNAs on cell surface[12], the imaging techniques with hybridization-mediated proximity ligation assay[26] and second-generation hierarchical coding strategy[27] for in situ visualization of cell surface glycoRNAs and the enrichment method for glycoRNAs[28] have been developed. The attachment site for N-glycans in glycoRNA[29] and they mediated neutrophil recruitment[30] and cell-

State Key Laboratory of Analytical Chemistry for Life Science, School of Chemistry, Nanjing University, Nanjing, China. ✉e-mail: ylc@nju.edu.cn; hxju@nju.edu.cn

penetrating peptide internalization[31] has been revealed. Besides, the glycoRNA in exosomes has also been discovered, which can facilitate intercellular communication through transfer to recipient cells[32] and enable sensitive cancer diagnostics[33]. Nevertheless, many issues about glycoRNAs, such as other types and distributions and components of glycoRNAs still remain unknown.

In this work, we design a general paradigm using Y RNAs as the object to achieve in situ identification of intracellular glycoRNAs from multiple perspectives. We firstly construct a fluorescence resonance energy transfer (FRET) system between glycan and RNA substrate by using general metabolic technique and bioorthogonal chemistry, which have been thought as powerful tools for the study of protein-associated glycans[34,35], to label fluorescence receptor to glycosyl groups of RNAs, and molecular recognition to bind fluorescence donor labelled DNA probe to RNA. The sensitive FRET signal demonstrates the presence of intracellular GlcNAcylated Y5 RNA, and indicates its distribution in nucleus by colocalization imaging. By collecting the target GlcNAc-RNA with magnetic beads (MBs) functionalized with DNA sequence complementing to Y5 RNA (MB-Cap-Y5), we identify the monosaccharide modified on RNA through gel electrophoresis analysis coupled with enzyme digestion, RNA sequencing and mass spectrometric analysis. Moreover, a GlcNAc-specific in situ hybridization-mediated proximity ligation assay (GlcISH-PLA) was developed to in situ quantify the GlcNAc-Y5 RNA with single-cell and single-molecule resolution. These findings innovate the distribution and quantitation information of glycoRNAs for promoting the functional research of glycoRNAs.

Results

FRET imaging of intracellular glycosylated Y5 RNA

The living HeLa cells were firstly metabolically labelled with Ac_4GlcNAz[36] or Ac_4ManNAz, respectively. To exclude the interference of glycoRNAs on cell surface, the labelled cells were treated with RNase A/T1 (RNase) (Fig. 1a), which was confirmed by subsequently incubating the cells with J2 antibody, which was reported to specifically recognize double-stranded Y5 RNA[37], and goat anti-mouse IgG AF488 antibody, and then being subjected to confocal laser scanning microscopic (CLSM) imaging. After RNase treatment, the cells showed negligible AF488 fluorescence (Supplementary Fig. 1), demonstrating the complete excising of the RNAs on cell membrane. The treated cells were then fixed with 4% paraformaldehyde (PFA) at 37 °C for 15 min and permeabilized with 0.25% Triton X-100 to facilitate the delivery of DBCO-Cy3 and following DNA probe into the cells. After delivering DBCO-Cy3 for the click reaction at 4 °C for 1 h, the GlcNAc or sialic acid (Sia) in cells was labelled by Cy3.

Afterward, the cells were incubated with FAM-DNA probe complementary to the sequence of Y5 RNA (Com-Y5-1) to recognize Y5 RNA. The excessive DBCO-Cy3 and Com-Y5-1 could be completely cleaned by simple washing with PBS, which was demonstrated by incubating the labelled HeLa cells with FAM labelled poly T DNAs (T84) and then thoroughly washing with PBS (Supplementary Fig. 2). The FRET from FAM as donor to Cy3 as acceptor could thus be performed to examine the presence of GlcNAc or Sia on intracellular Y5 RNA.

All the metabolically labelled cells treated with DBCO-Cy3 and Com-Y5-1 exhibited obvious Cy3 and FAM fluorescence inside cells, while these without metabolic labeling as control did not exhibit Cy3 fluorescence (Fig. 1b), which indicated the successful metabolic labelling of GlcNAc and Sia, and the hybridization of intracellular Y5 RNA with Com-Y5-1, and excluded nonspecific adsorption of DBCO-Cy3 inside cells. The tiny Cy3 signal from Ac_4ManNAz-treated cells resulted from the presence of few Sia inside cells and the effects of PFA fixation and permeabilization treatments on cell surface Sia. The latter led to great decrease of Cy3 fluorescence on Ac_4ManNAz-treated cell surface (Supplementary Fig. 3). Interestingly, RNase treatment hardly influenced the Cy3 signal on cell surface. These phenomena were beneficial to the investigation of GlcNAcylation inside cells.

The FRET signal could be collected in 550–600 nm for Cy3 with the excitation wavelength of 488 nm from FAM. The Ac_4GlcNAz metabolically labelled cells exhibited obvious FRET signal (Fig. 1b), which was not observed from both Ac_4ManNAz-treated cells (Fig. 1c) and the control, indicating the presence of GlcNAc-Y5 RNA and that the intracellular glycoRNAs did not contain Sia. Notably, the reduced FAM intensity and tiny Cy3 intensity may be caused by the close spatial proximity of sialylated molecules to Y5 RNAs inside cells or the presence of intracellular sialoglycoRNAs. In the magnified images of HeLa cells (Supplementary Fig. 4), the FRET signals were enriched in several spots and highly overlapped with the FAM signals, while the Cy3 signal exhibited a relatively uniform distribution, which indicated that most Y5 RNAs were modified with GlcNAc and exhibited a spots-clustered distribution inside cells.

To demonstrate the specificity of FRET signal, we respectively knocked out the Y5 RNA in HeLa cells by CRISPR/Cas9[29] and inhibited GlcNAc by 6-Diazo-5-oxo-L-norleucine (DON), which can suppress glutamine fructose-6-phosphate amidotransferase to deplete UDP-GlcNAc levels[38,39]. After performing the FRET imaging procedure (Fig. 1a), the FAM and FRET signals in the Y5 knocked out cells disappeared, while the Cy3 signals remained (Supplementary Fig. 5). In contrast, the Cy3 and FRET signals in the DON treated cells disappeared, while the FAM signals remained (Supplementary Fig. 5). These phenomena demonstrated that the FRET signal was specifically initiated from the GlcNAc-Y5 RNA.

To exclude the possible false-positive FRET signal caused by the glycosylated RNA-binding proteins, a Cy3-modified Ro60 antibody (AntiRo60-Cy3) was used to label the Ro60 proteins inside HeLa cells, which was reported to interact with the double-stranded region of Y RNAs hairpin[40]. After incubated with Com-Y5-1, the AntiRo60-Cy3 treated HeLa cells exhibited obvious FAM and Cy3 fluorescence but no FRET signals (Supplementary Fig. 6a). Meanwhile, the Anti60 pre-treated HeLa cells were also incubated with AntiRo60-Cy3 and then Com-Y5-1, which exhibited similar FAM fluorescence but tiny Cy3 fluorescence (Supplementary Fig. 6a). These phenomena indicated the specific recognition of AntiRo60-Cy3 to Ro60 proteins inside cells, and the fluorescence acceptor bound on the RNA-binding proteins could not initiate the FRET with the donor bound on the RNA, which were too far away from each other. To further exclude the influence of any potential RNA-binding proteins including Ro60, the HeLa cells were incubated with NHS-Cy3 to directly label any proteins of cells (Supplementary Fig. 6b). To investigate whether the direct incubation of NHS-Cy3 with cells could label the intracellular Ro60 protein, the Ro60 protein was extracted from the lysates of NHS-Cy3 incubated cells by AntiRo60 bound magnetic beads and subjected to Sodium Dodecyl Sulfate-Polyacrylamide gel electrophoresis (SDS-PAGE) analysis (Supplementary Fig. 6c, d). The extracted Ro60 protein exhibited a distinct band at the correct molecular weight position (Supplementary Fig. 6c) and emitted strong Cy3 fluorescence under excitation (Supplementary Fig. 6d), which indicated the direct incubation of N-hydroxysuccinimide Cy3 ester (NHS-Cy3) with cells could label Ro60. Subsequently, the RNase-treated HeLa cells were sequentially incubated with Com-Y5-1 and NHS-Cy3 and subjected to CLSM imaging (Supplementary Fig. 6e). The CLSM images exhibited obvious FAM and Cy3 fluorescence, but no FRET signals (Supplementary Fig. 6f), and the overlapped FAM and Cy3 fluorescence in the magnified images exhibited no FRET signals (Supplementary Fig. 6g), which further demonstrated that the proteins whether nor RNA-binding proteins cannot bring false-positive FRET signal.

To estimate the modification site of GlcNAc on Y5 RNA, another seven FAM-DNA probes (Com-Y5-2 to Com-Y5-8) with the FAM labelling positions different from Com-Y5-1 was used to recognize the Y5

https://doi.org/10.1038/s41467-026-72909-4

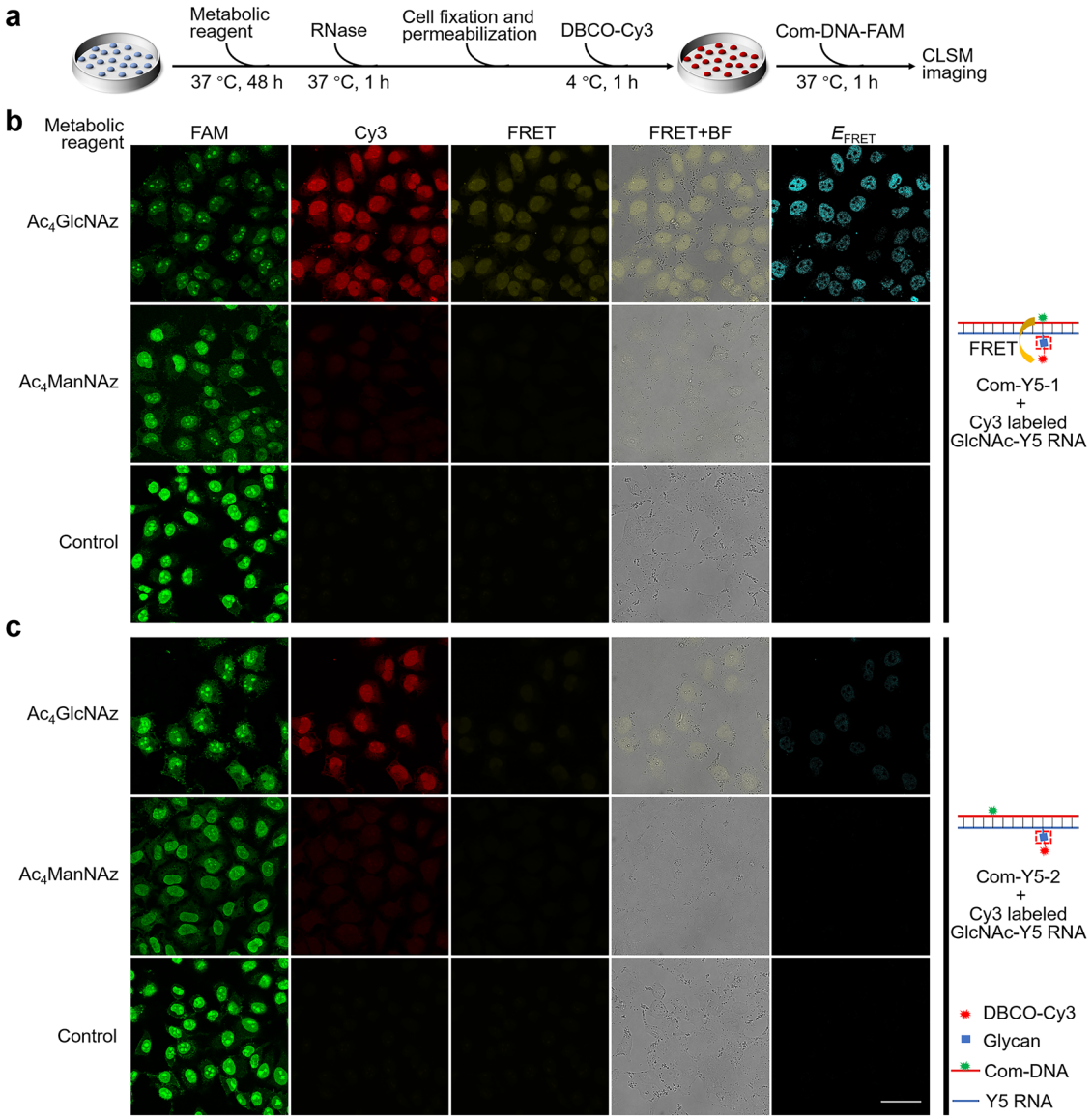

Fig. 1 | FRET imaging of intracellular GlcNAc-Y5 RNA in HeLa cells. a Schematic diagram of the procedure for imaging of intracellular GlcNAc-Y5 RNA by FRET. **b** CLSM images of HeLa cells after performing metabolic labelling with $Ac_4GlcNAz$ or $Ac_4ManNAz$, RNase treatment, PFA fixation, permeabilization treatment, DBCO-Cy3 incubation and Com-Y5-1 recognition. **c** CLSM images of HeLa cells after sequentially treated with the same procedure as (**b**), replacing Com-Y5-1 by Com-Y5-2. Control means without metabolic reagent treatment. FAM channel was collected in 500–550 nm with λ_{ex} = 488 nm of FAM-DNA probes. Cy3 channel was collected in 550–600 nm with λ_{ex} = 520 nm of DBCO-Cy3. FRET channel was collected in 550–600 nm with λ_{ex} = 488 nm. $E_{FRET} = I_{FRET}/I_{FAM\ as\ donor}$. Each experiment was repeated 3 times independently with similar results. Scale bar, 50 μm.

RNA (Supplementary Fig. 7a). As a result, only the cells treated with Com-Y5-5 exhibited obvious FRET signal, which had the closest FAM labelling position comparing to Com-Y5-1 (Fig. 1c and Supplementary Fig. 7b). The much weaker FRET signals in other FAM-DNA probes treated cells were due to the farther distance between the fluorescence donor and acceptor[41,42], which indicated the GlcNAc modification site was close to the complementary positions of Com-Y5-1 and Com-Y5-5. Subsequently, the Com-Y5-1 and Com-Y5-2 were selected as the representatively positive and negative probes for other cell lines due to their middle-located FAM labelling positions.

The FRET approach was further used to explore the possible presence of intracellular GlcNAc-Y5 RNA in HaCaT, MCF-7 and MCF-10A cells. Similar results were observed in these cell lines (Supplementary Figs. 8–10), and the cells treated with Com-Y5-1 all exhibited higher FRET signals than those treated with Com-Y5-2, indicating the closer distance from the modification site of GlcNAc on Y5 RNA to FAM on Com-Y5-1. This preliminary validation provided the evidence of GlcNAc-Y5 RNA existing inside cells.

Distribution of GlcNAc-Y5 RNA in cells

The distribution of GlcNAc-Y5 RNA in cellular organelles was studied by colocalization analysis. After the Cy3 labelled HeLa cells were treated with Com-Y5-1, they were further incubated with ER-Red, Golgi-Red, or Hoechst 33342 to stain the endoplasmic reticulum (ER), Golgi apparatus or nucleus (Fig. 2a)[43,44]. These dyes possess different excitation and fluorescence emission ranges compared to FAM and Cy3 (Supplementary Fig. 11). Their fluorescence images can thus be collected for examining the distribution of GlcNAc-Y5 RNA in cells. From the FAM images and their merged images with ER-Red, Golgi-Red, or Hoechst 33342 images of these cells (Fig. 2b–d and Supplementary Fig. 12), it could be concluded that Y5 RNA mainly distributed in nucleus, which was identical to the previous report[45]. Other merged

https://doi.org/10.1038/s41467-026-72909-4

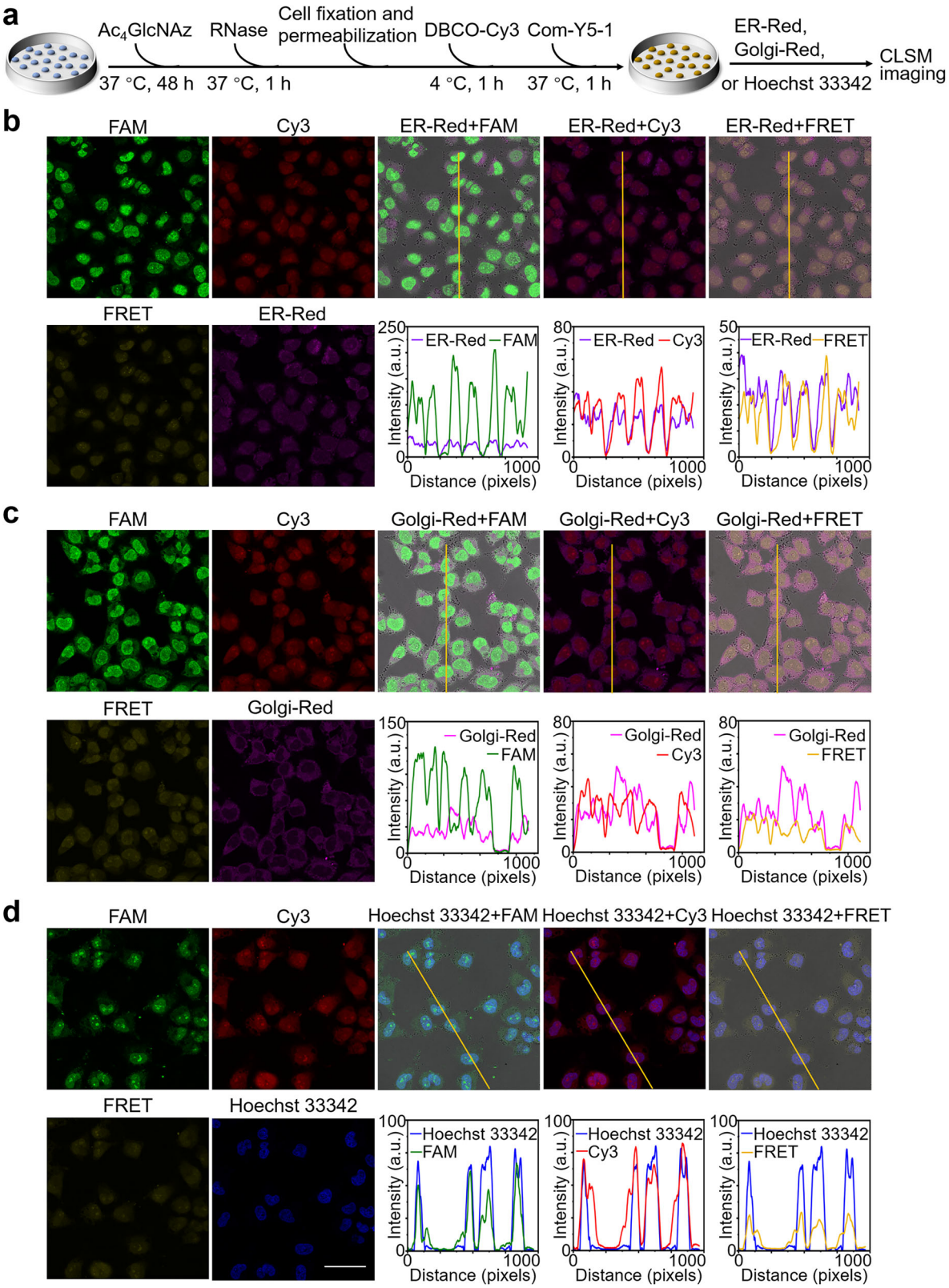

images showed the difference of fluorescence peak positions of FAM from ER-Red or Golgi-Red. In the magnified images (Supplementary Fig. 13), it could be obviously observed that the Golgi-Red and ER-Red exhibited characteristic distributions but little overlap with the FRET signal. Interestingly, the Cy3 images of all the four cell lines exhibited higher colocalization coefficients with both ER and nucleus (Fig. 2b and d), and lower colocalization coefficient with Golgi apparatus (Fig. 2c and Supplementary Figs. 14–16), which demonstrated GlcNAc had a broad distribution inside cells. Notably, the FRET images from nucleus exhibited higher colocalization coefficient (with a Pearson's coefficient of 0.872 ± 0.113) (Fig. 2d), and the lower colocalization coefficients occurred in ER-Red (with a Pearson's coefficient of 0.328 ± 0.153) and Golgi-Red (with a Pearson's coefficient of 0.465 ± 0.120) treated cells (Fig. 2b, c and Supplementary Figs. 14–16),

Fig. 2 | Colocalization imaging of intracellular GlcNAc-Y5 RNA in HeLa cells. **a** Schematic diagram of the procedure for colocalization imaging of intracellular GlcNAc-Y5 RNA. **b** CLSM images of HeLa cells after performing metabolic labelling with Ac_4GlcNAz, RNase treatment, PFA fixation, permeabilization treatment, DBCO-Cy3 incubation, Com-Y5-1 recognition, and then incubation with 500 nM ER-Red in Hanks for 20 min at 37 °C, along with FAM, Cy3 and FRET channel colocalization analysis. **c** CLSM images of HeLa cells after treated with the same procedure as (**b**), replacing ER-Red by Golgi-Red in Hanks at 1:100 dilution for 30 min at 4 °C, along with FAM, Cy3 and FRET channel colocalization analysis. **d** CLSM images of HeLa cells after treated with the same procedure as (**b**), replacing ER-red by 10 μg/mL Hoechst 33342 for 10 min at room temperature, along with FAM, Cy3 and FRET channel colocalization analysis. The images were collected in 500–550 nm with λ_{ex} = 488 nm for FAM, 550–600 nm with λ_{ex} = 520 nm for Cy3 and 488 nm for FRET, 420–500 nm with λ_{ex} = 405 nm for Hoechst 33342, 600–670 nm with λ_{ex} = 587 nm for ER-Red and Golgi-Red. Each experiment was repeated 3 times independently with similar results. Scale bar, 50 μm.

further demonstrating the main distribution of GlcNAc-Y5 RNA inside nucleus. As a negative control, the Ac_4ManNAz metabolic labelled cells were also subjected to colocalization analysis. They showed very weak Cy3 and FRET fluorescence, as observed in Supplementary Fig. 3, and did not exhibit any colocalization coefficient with ER, Golgi apparatus and nucleus (Supplementary Fig. 17).

Verification of intracellular GlcNAc-Y5 RNA

To verify the existence of intracellular GlcNAc-Y5 RNA, we designed a target-specific approach to collect the Y5 RNAs (Fig. 3a). Firstly, the total RNAs from the metabolically labelled and then RNase-treated HeLa cells were extracted with a traditional procedure using Trizol reagent[46]. The target Y5 RNA was then collected with MB-Cap-Y5 from the total intracellular RNAs by specific hybridization of Y5 RNA with Cap-Y5. After the intracellular Y5 RNA collected on MB-Cap-Y5 was incubated with DBCO-FAM, obvious FAM fluorescence was observed on the MB surface (Fig. 3b), while the MB-Cap-Y5 and the controls exhibited negligible FAM fluorescence after reaction with DBCO-FAM. Here, the controls were prepared by incubating MB-Cap-Y5 with the extracts from un-labelled or Ac_4ManNAz metabolically labelled HeLa cells, or incubating MB-Ran with total RNA extract from metabolically labelled cells, respectively. These phenomena indicated the presence of GlcNAc on intracellular Y5 RNA from HeLa cells. Other cells, such as HaCaT, MCF-7 and MCF-10A cells showed the similar phenomena (Supplementary Fig. 18), demonstrating the GlcNAcylation of intracellular Y5 RNA. To explore the component of intracellular GlcNAc-Y5 RNA, the Y5 RNA was collected from un-labelled HeLa cells and then released from the MBs with a release DNA (Rel-Y5) completely complementary to Cap-Y5 (Fig. 3c) to perform gel electrophoresis (PAGE) analysis. A synthetic Y5 RNA (Syn-Y5) without any modification was used as control. The specific capture of Y5 RNA by MB-Cap-Y5 was firstly demonstrated with random sequenced DNA modified MBs (MB-Cap-R1) and corresponding release DNA (Rel-R1), which did not show any band after performing the same procedure as that for Y5 RNA collection from the cells (Supplementary Fig. 19a and Fig. 3d). The displacement of Y5 RNA captured on the MBs by Cap-Y5 was also verified by a new band after incubating Cap-Y5 and Rel-Y5 (Supplementary Fig. 19b). The obtained Y5 RNA exhibited a distinct band at a position with lower mobility or greater molecular weight than Syn-Y5 (Fig. 3d, Lanes 3 and 4), indicating that the Y5 RNA from the cells contained additional modifications. After Ac_4GlcNAz metabolic labelling, the released Y5 RNA from the cells exhibited similar location to that from the un-labelled cells (Lanes 2 and 3) due to the small molecular weight of labelled -N_3, which led to strong FAM fluorescence after the reaction with DBCO-FAM (Fig. 3e). This result along with the PAGE analysis of the intracellular Y5 RNA from HaCaT, MCF-7 and MCF-10A cells (Supplementary Fig. 20) further validated the existence of GlcNAc on intracellular Y5 RNA.

To exclude the possible fault results of the PAGE analysis, we incubated the released Y5 RNA from un-labelled HeLa cells with Ac_4GlcNAz, which showed the same band as that of the Y5 RNA from Ac_4GlcNAz labelled cells, but weaker FAM fluorescence after further incubating with DBCO-FAM (Supplementary Fig. 21). Moreover, the in vitro labelling needed much higher concentration of Ac_4GlcNAz, which was agreed with the reported adverse effects[47], and ensured the reliability of the results obtained at low Ac_4GlcNAz concentration.

Enzymatic validation of intracellular Y5 RNA components

To explore the components of intracellular glycosylated Y5 RNA, we used RNase and different glycosidases to treat the labelled cells and the extracted Y5 RNA samples. After the Cy3 labelled HeLa cells were treated with Com-Y5-1, the cells were further incubated with β-N-acetylglucosaminidase S (GlcNAcase)[48], O-glycosidase[49] or PNGase F[50] (Fig. 4a). All glycosidase-treated cells showed strong FAM fluorescence from hybridized Com-Y5-1, which were similar to the control (Fig. 4b, c), indicating that the glycosidases treatment did not influence the nucleic acid chain of Y5 RNA. However, GlcNAcase treatment led to significant disappearance of the E_{FRET} intensity, while these of O-glycosidase and PNGase F treated cells did not show obvious change (Fig. 4d). To demonstrate the selectivity of the glycan labeling, the total intracellular RNA samples from Ac_4GlcNAz labeled and RNase digested HeLa cells were also treated with GlcNAcase, O-glycosidase or PNGase F and then followed with DBCO-FAM incubation and agarose gel electrophoresis analysis (Supplementary Fig. 22). Only the GlcNAcase-treated sample exhibited the loss of the fluorescence signal, which indicated the selective labeling of GlcNAc monosaccharide on intracellular RNAs by Ac_4GlcNAz. Meanwhile, after treating the Y5 RNA collected MB-Cap-Y5 with GlcNAcase, O-glycosidase or PNGase F and then incubated with DBCO-FAM, the FAM fluorescence on GlcNAcase-treated MBs disappeared while these on O-glycosidase and PNGase F-treated MBs remained unchanged (Supplementary Fig. 23). These results indicated the presence of GlcNAc monosaccharide and the insignificant existence of N- or O- glycans on intracellular Y5 RNA.

As negative control, the Ac_4ManNAz metabolic labelled HeLa cells showed the presence of few Sia and negligible FRET signal (Supplementary Fig. 24), indicating that the Sia was not on Y5 RNA. After the cells were further treated with glycosidases, only PNGase F treatment led to weaker Cy3 fluorescence (Supplementary Fig. 24c), demonstrating the degradation of the Sia-terminated N-glycans from intracellular glycoproteins.

After the Y5 RNA sample from Ac_4GlcNAz and RNase treated HeLa cells was incubated with GlcNAcase, it showed a distinct PAGE band at a position with slightly higher mobility of lower molecular weight than other glycosidase incubated samples (Fig. 4f). Only this band was invisible after the samples were incubated with DBCO-FAM and then different glycosidases to be loaded into the gel, respectively (Fig. 4g), indicating efficient GlcNAcase digestion[48], and thus further demonstrating the GlcNAc monosaccharide modification of Y5 RNA.

As the GlcNAc monosaccharide generally links to the proteins at the specific amino acids, we investigated the possible amino acid linkage between GlcNAc monosaccharide and RNA by using the proteinase K (Pro. K), which can degrade the serine amino acid linkages[12]. After the Y5 RNA sample from HeLa cells and Syn-Y5 was incubated with protease-K, no band shift was observed (Supplementary Fig. 25), which indicated the GlcNAc monosaccharide on Y5 RNA did not link to any amino acids.

The designed glycosidases-based strategy was also performed to validate the intracellular Y5 RNA components in HaCaT, MCF-7 and MCF-10A cells. All these cell lines showed the same CLSM imaging and PAGE results (Supplementary Figs. 26–32), demonstrating the universality of GlcNAc monosaccharide modification of intracellular Y5 RNA.

https://doi.org/10.1038/s41467-026-72909-4

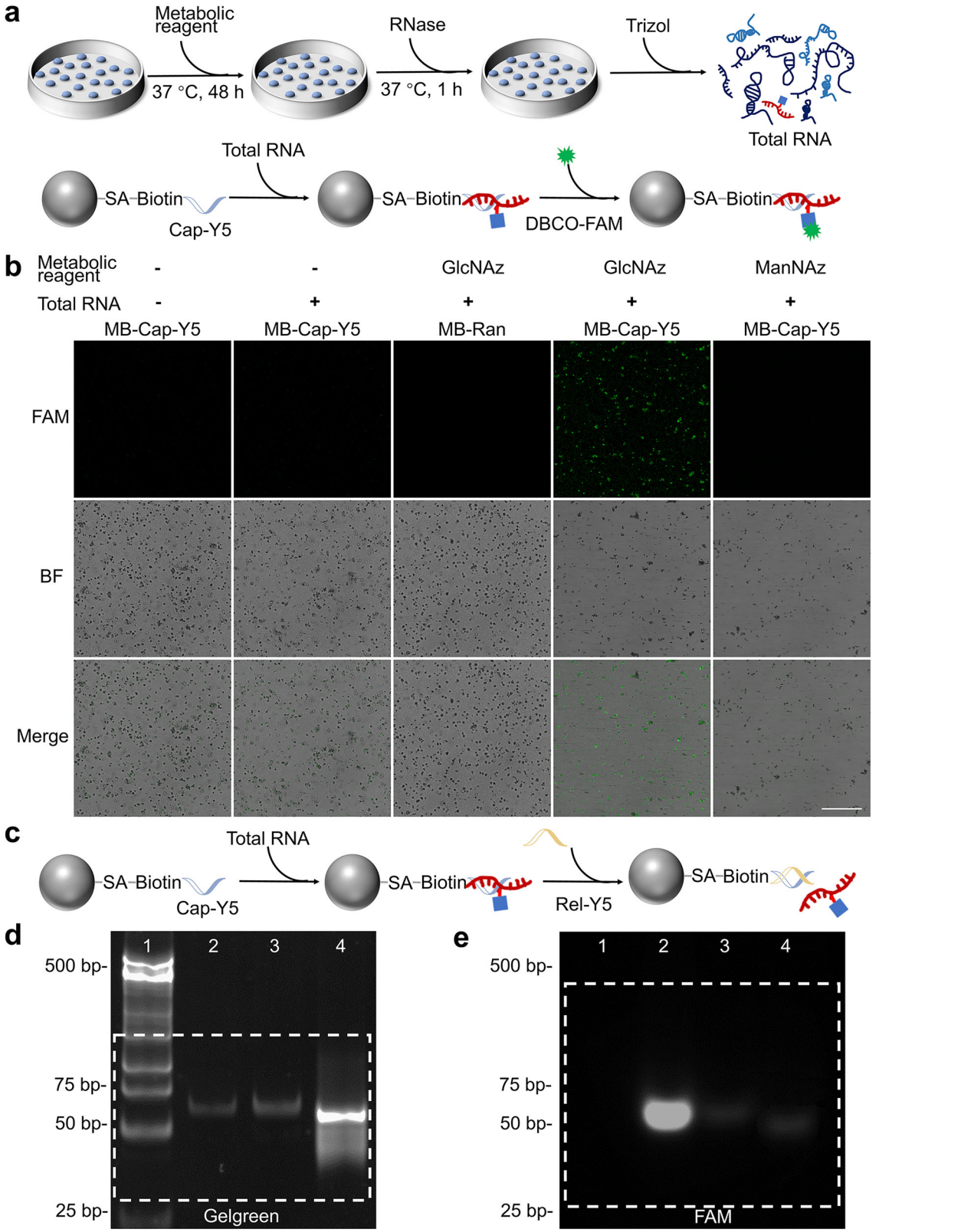

Fig. 3 | Collection and verification of GlcNAc-Y5 RNA from cells. a Schematic diagram of the extraction of total RNAs from cells and the collection and identification of GlcNAc-Y5 RNA from total RNAs. **b** CLSM images of MBs incubated with Cap-DNAs, then incubated with total RNA from 40 μM Ac_4GlcNAc or Ac_4ManNAz-treated HeLa cells, and then treated with 100 μM DBCO-FAM at 4 °C for 1 h. The images were collected in 500–550 nm with λ_{ex} = 488 nm for FAM. Each experiment was repeated 3 times independently with similar results. Scale bar, 50 μm. **c** Schematic diagram of the release of GlcNAc-Y5 RNA from MB-Cap-Y5. **d** PAGE analysis. Lane 1: marker, Lane 2: Y5 RNA from Ac_4GlcNAz metabolically labelled and RNase treated HeLa cells, Lane 3: Y5 RNA from RNase treated HeLa cells, and Lane 4: Syn-Y5. **e** Fluorescence images of the gel (**d**) after treating all lanes with 100 μM DBCO-FAM at 4 °C for 1 h.

https://doi.org/10.1038/s41467-026-72909-4

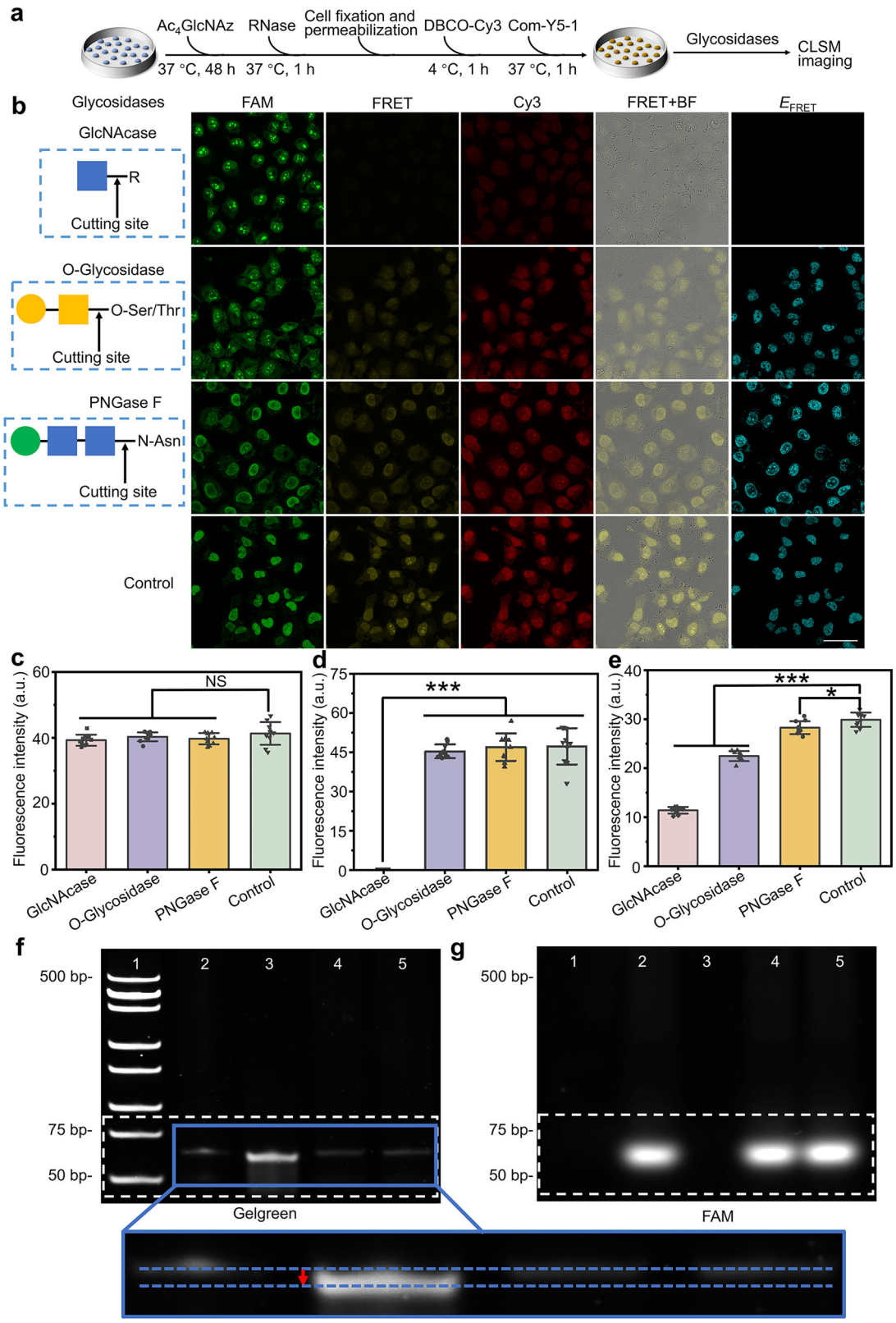

GlcNAc modification of other intracellular RNAs

The possibility of GlcNAc modification of other intracellular Y RNAs was investigated using Y3 and Y4 RNAs as the candidates[51,52], and Com-Y3-DNA and Com-Y4-DNA for RNA labelling. Different from Com-Y5-DNA labelling, both Com-Y3-DNA and Com-Y4-DNA labelled cells did not exhibit FRET signal, though the strong FAM fluorescence could be observed (Fig. 5a), indicating the presence of Y3 and Y4 RNA, and the absence of GlcNAc. Thus, both Y3 and Y4 RNAs were not modified with GlcNAc. This conclusion was also confirmed by PAGE analysis after Y3 and Y4 RNAs were collected from the cells with corresponding Cap-Y3-DNA, Rel-Y3-DNA, Cap-Y4-DNA and Rel-Y4-DNA probes, which showed the same hybridization and displacement behaviors (Supplementary Figs. 33 and 34). Compared to those for Y5 RNA, the extracted Y3 and Y4 RNAs exhibited the bands at slightly different positions due to the

Fig. 4 | Identification of Y5 RNA components in HeLa cells treated with $Ac_4GlcNAz$. **a** Schematic diagram of the procedure for identification of the monosaccharides on Y5 RNA by glycosidases. **b** CLSM images of Y5 RNA in HeLa cells after performing metabolic labelling with $Ac_4GlcNAz$, RNase treatment, PFA fixation, permeabilization treatment, DBCO-Cy3 incubation, Com-Y5-1 recognition, and then incubation with 400 U/mL GlcNAcase at 37 °C for 1 h, 4000 kU/mL O-Glycosidase at 37 °C for 3 h or 25 kU/mL PNGase F at 37 °C for 1 h. Control means without glycosidase treatment. The images were collected in 500–550 nm with λ_{ex} = 488 nm for FAM, 550–600 nm with λ_{ex} = 520 nm for Cy3 and 488 nm for FRET. $E_{FRET} = I_{FRET}/I_{FAM\ as\ donor}$. Scale bar, 50 μm. **c**–**e** Histograms and statistical analysis of the fluorescence intensities of single cell from **c** FAM channel, **d** E_{FRET} channel, and **e** Cy3 channel in (**b**). Data were presented as mean values ± SD. Statistical analysis was performed by unpaired two-tailed *t*-tests (*$p < 0.05$; **$p < 0.005$; ***$p < 0.0005$; NS, not significant), $n = 10$. The *p*-values are as follows: **c** GlcNAcase *vs* O-Glycosidase, $p = 0.112$; O-Glycosidase *vs* Control, $p = 0.403$; PNGase F *vs* Control, $p = 0.213$. **d** GlcNAcase *vs* O-Glycosidase, $p = 1.31 \times 10^{-12}$; GlcNAcase *vs* PNGase F, $p = 4.04 \times 10^{-10}$; GlcNAcase *vs* Column 4, $p = 4.70 \times 10^{-9}$. **e** GlcNAcase *vs* Control, $p = 3.62 \times 10^{-14}$; O-Glycosidase *vs* Control, $p = 1.13 \times 10^{-10}$; PNGase F *vs* Column 4, $p = 0.018$. **f** PAGE analysis of the Y5 RNA from $Ac_4GlcNAz$ metabolically labelled and RNase-treated HeLa cells, after incubated with 400 U/mL GlcNAcase at 37 °C for 1 h, 4000 kU/mL O-Glycosidase at 37 °C for 3 h or 25 kU/mL PNGase F at 37 °C for 1 h. Lane 1: marker, Lane 2: extracted Y5 RNA, Lane 3–5: extracted Y5 RNA after incubated with GlcNAcase (3), PNGase F (4), and O-Glycosidase (5). **g** Fluorescence images of the gel **(f)** after treating all lanes with 100 μM DBCO-FAM at 4 °C for 1 h.

different sequences of RNAs (Fig. 5b, Lanes 2, 5 and 8). After the extracted Y3, Y4 and Y5 RNAs were incubated with RNase, their bands disappeared, while the incubation with the mixture of RNase and RNase inhibitor could remain these bands at corresponding locations (Fig. 5b, Lanes 3, 4, 6, 7, 9 and 10), indicating that the extracted nucleic acids were exactly RNAs. Moreover, after these RNAs samples were reacted with DBCO-FAM, and then treated with RNase or the mixture of RNase and RNase inhibitor to perform the PAGE analysis, only the bands of Y5 RNA and its sample after treated with the mixture of RNase and RNase inhibitor showed strong FAM fluorescence (Fig. 5c, Lanes 2 and 4), which came from the labelled GlcNAc, further demonstrating the absence of GlcNAc in Y3 and Y4 RNAs.

To further investigate the existence of other intracellular GlcNAc-modified RNAs, total intracellular RNAs from the $Ac_4GlcNAz$ metabolically labelled and then RNase-treated HeLa cells were extracted with the traditional procedure using Trizol reagent, which exhibited similar bands distribution on agarose gel comparing to the only RNase-treated HeLa cells but strong FAM fluorescence after incubated with DBCO-FAM (Supplementary Fig. 35), indicating the GlcNAc in total intracellular RNAs. The azide-containing RNAs were collected and enriched through copper-catalyzed click chemistry with alkyne-biotin and streptavidin magnetic beads. After streptavidin elution and immunoprecipitation, the RNA samples were subjected to PANDORA-seq library construction and sequencing. According to the sequencing results (Supplementary Fig. 36), many other RNAs, including tRNA-derived small RNAs, snoRNAs, piRNA clusters, and specific microRNAs were modified with GlcNAc.

To investigate the sensitivity of the FRET imaging for intracellular glycoRNAs, the hsa-miR-140-3p with low expression and GlcNAcylation levels was selected for FRET imaging. After performing the same FRET imaging procedure by using the FAM labelled Com-miR-140-3p probe, obvious FRET signal was observed (Supplementary Fig. 37), which demonstrated the capability of the designed FRET imaging procedure to study the existence of glycoRNAs with low expression or GlcNAcylation levels.

Identification of GlcNAc-Y5 RNA by mass spectrometric analysis

Matrix-assisted laser desorption/ionization-time of flight (MALDI-TOF) and higher-resolution Orbitrap Eclipse Tribrid mass spectrometric analysis are powerful tools to determine the components of biological molecules[53,54]. Using 3-hydroxypicolinic acid (HPA) as matrix[55], we firstly confirmed the presence of GlcNAc on intracellular Y5 RNA (Fig. 6a). Four RNA ribonucleotides exhibited distinct peaks at m/z of 322.4 for CMP, 323.5 for UMP, 346.4 for AMP, and 362.5 for GMP ($[M\text{-}H]^-$), respectively (Supplementary Fig. 38 i, ii). Compared to the mass spectra of the mixture of RNase and RNase treated Syn-Y5 (Fig. 6b and Supplementary Fig. 38 iii, iv), the GMP peak could be used to identify the degraded RNA, which occurred in the mass spectra of all RNase treated intracellular Y5 RNA from HeLa, HaCaT, MCF-7 and MCF-10A cells (Supplementary Fig. 38 v–viii), indicating the successful degradation of the Y5 RNA. Interestingly, extra peaks at m/z of 537.481, 537.484, 537.489 and 537.487 were observed from RNase-treated intracellular Y5 RNA from HeLa, HaCaT, MCF-7 and MCF-10A cells, respectively by using the higher-resolution Orbitrap Eclipse Tribrid mass spectrometer (Fig. 6b, v and Supplementary Fig. 39), which was absent in the spectrum of RNase-treated Syn-Y5 (Fig. 6b, iv). Thus, this extra peak was possibly attributed to the GlcNAc-modified ribonucleotide. To explore the source, the Y5 RNA samples extracted from $Ac_4ManNAz$ or $Ac_4GlcNAz$ metabolically labelled HeLa and HaCaT cells were treated with RNase for mass spectrometric analysis. The mass spectra from $Ac_4ManNAz$-treated cells remained the peak at m/z of 537.5, as that from un-labelled cells, while $Ac_4GlcNAz$ labelling led to a new peak at m/z of 578.483 and 578.486, and the disappearance of the peak at m/z of 537.481 and 537.484 for HeLa and HaCaT cells (Fig. 6c and Supplementary Fig. 40), respectively. These results excluded the presence of Sia in intracellular Y5 RNA again, and demonstrated the successful metabolic labelling process by replacing the GlcNAc monosaccharide with GlcNAz containing an extra azide group (m.w. ~41) (Supplementary Fig. 41)[11,56], which coincidentally matched the peak shifts of 41.002 from 537.481 to 578.483 and 537.484 to 578.486, respectively.

The GlcNAc monosaccharide modification of Y5 RNA was further verified by glycosidases digestion and then RNase degradation. GlcNAcase digestion of the intracellular Y5 RNAs from four different cells led to the disappearance of the peak at m/z of 537.5, while O-Glycosidase or PNGase F digestion did not change the peak at m/z of 537.5 (Fig. 6d and Supplementary Fig. 42).

Next, we investigated the modification site of GlcNAc on intracellular Y5 RNA with mass spectrometric analysis in negative linear mode. The feasibility for detecting GlcNAc-ribonucleotide was demonstrated with the commercialized UDP-GlcNAc (607.4), which showed a strong peak at m/z of 606.6 ($[M\text{-}H]^-$) (Supplementary Fig. 43). Considering that RNase cannot divide the connections on the AMP 3′ side[57], we checked the cleavage performance of RNase to other 3′ sides by incubating 5′-AUAUAU-3′, 5′-AGAGAG-3′ and 5′-ACACAC-3′ with RNase for MALDI-TOF analysis, which showed the peaks at m/z of 652.5, 691.7 and 651.5, respectively (Supplementary Fig. 44). These peaks were attributed to AU, AG, and AC structures ($[M\text{-}H]^-$), respectively. After the comparison with the RNA modification database (Modomics, https://genesilico.pl/modomics/modifications), the m/z of 537.5 could not match with any known single ribonucleotide carrying modifications. Thus, the peak at m/z of 537.5 from the Y5 RNAs was possibly attributed to a dual-ribonucleotides structure containing AMP or its derivative.

To detail the GlcNAc-modified ribonucleotide component, MS/MS analysis was performed by collecting the peak of Y5 RNA at m/z of 537.5, which showed a new peak at m/z of 396.4 for all the studied cells (Supplementary Fig. 45). Besides, peaks at m/z around 1075.96 were simultaneously observed from RNase treated intracellular Y5 RNA of HeLa, HaCaT, MCF-7 or MCF-10A cells under a broad detection range by the higher-resolution Orbitrap Eclipse Tribrid mass spectrometer (Supplementary Fig. 46), which was twice of the peaks around m/z of 537.48 after plus one hydrogen mass. As the isotopic peaks of m/z of 537.48 located around 537.98 with peak shifts of 0.5 (Supplementary Fig. 47), it was reasonable to deduce that the peaks around m/z of

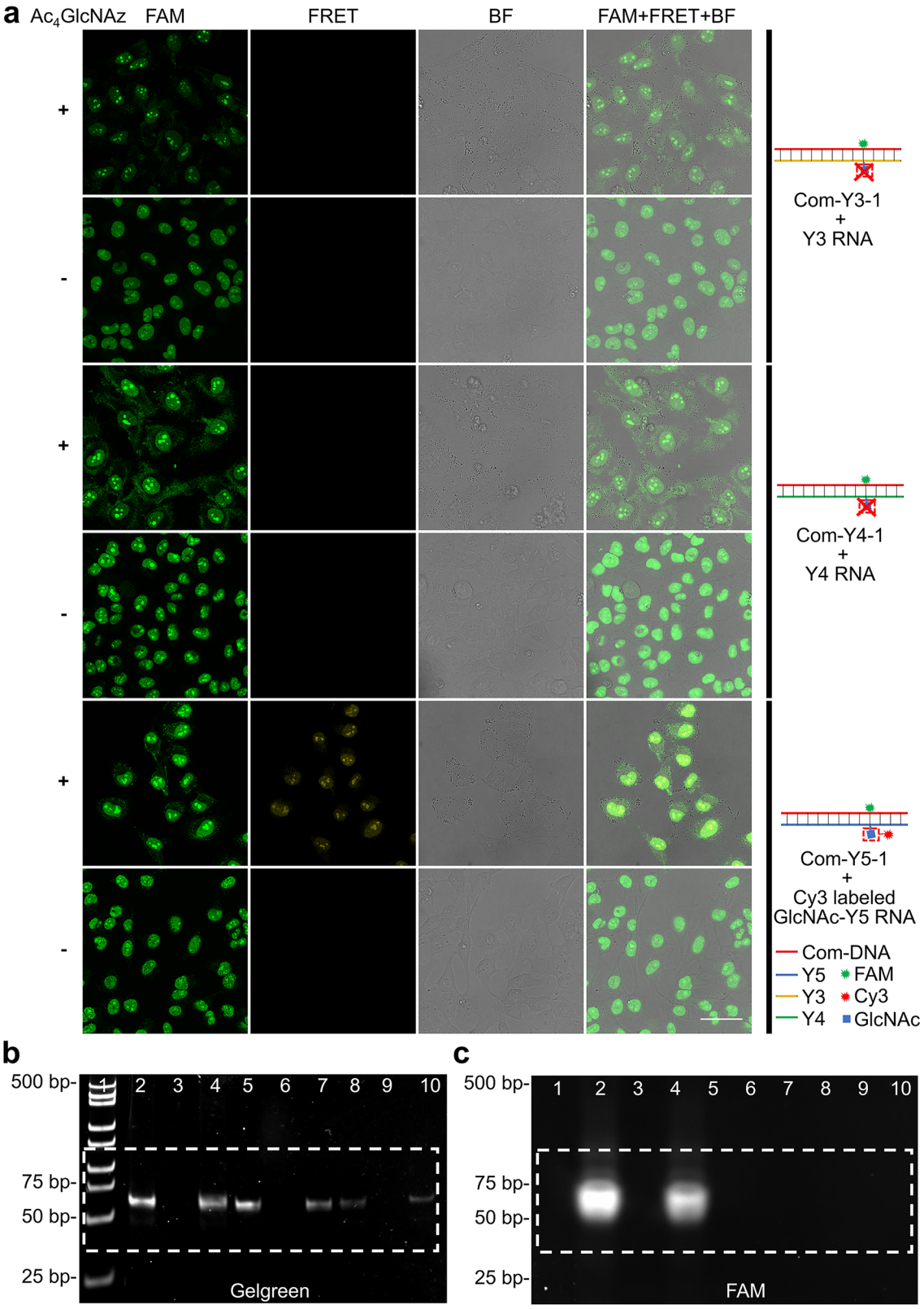

1075.96 ([M-H]$^-$) were the singly charged version of the conjugate of GlcNAc and ribonucleotides, while the peaks around m/z of 537.48 ([M-2H]$^{2-}$) arose from the loss of two hydrion[58,59].

In situ quantification of GlcNAc-Y5 RNA by GlcISH-PLA

Since the existence of GlcNAc-Y5 RNA has been demonstrated, we finally quantitatively assessed the level of GlcNAc-Y5 RNA in situ in single cell by GlcISH-PLA using STED super-resolution imaging. In situ hybridization-mediated proximity ligation assay (ISH-PLA) is a powerful method to quantify the intracellular RNA modification, which has been applied to in situ imaging of Sia-modified RNA (ARPLA) on cell surface[26] and m6A modification of mRNA inside cells[60]. The ARPLA utilized an aptamer to recognize Sia, which exhibited advantages of pre-labeling-free and broad glycan targets. Considering of the

Fig. 5 | GlcNAc modification on the other Y RNAs in HeLa cells. a CLSM images of HeLa cells after performing metabolic labelling with Ac_4GlcNAz, RNase treatment, PFA fixation, permeabilization treatment, DBCO-Cy3 incubation, and Com-Y3-1 or Com-Y4-1 recognition. The images were collected in 500–550 nm with λ_{ex} = 488 nm for FAM, and 550–600 nm with λ_{ex} = 520 nm for Cy3 and 488 nm for FRET. Each experiment was repeated 3 times independently with similar results. Scale bar, 50 μm. **b** PAGE analysis of Y3, Y4 and Y5 RNAs from Ac_4GlcNAz metabolically labelled and RNase treated HeLa cells after incubation with RNase in absence or presence of 4000 U/mL RNase Inhibitor at 37 °C for 1 h. Lane 1: marker, Lane 2: extracted Y5 RNA, Lanes 3, 4: extracted Y5 RNA after incubated with RNase (3) and the mixture of RNase and RNase Inhibitor (4), Lane 5: extracted Y3 RNA, Lanes 6, 7: extracted Y3 RNA after incubated with RNase (6) and the mixture of RNase and RNase Inhibitor (7), Lane 8: extracted Y4 RNA, Lanes 9, 10: extracted Y4 RNA after incubated with RNase (9) and the mixture of RNase and RNase Inhibitor (10). **c** Fluorescence images of the gel (**b**) after treating all lanes with 100 μM DBCO-FAM at 4 °C for 1 h.

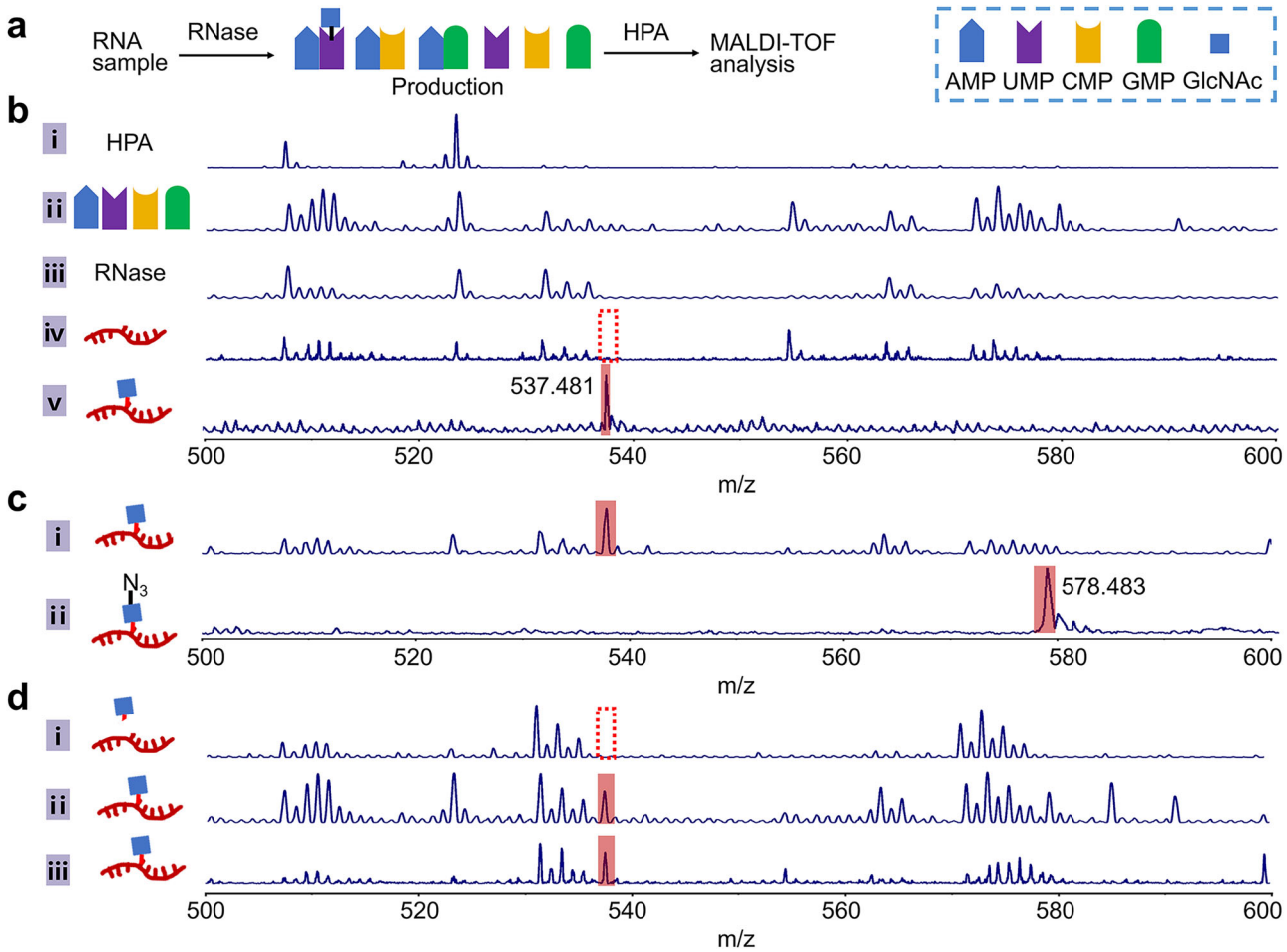

Fig. 6 | Mass spectrometric analysis of GlcNAc modification site on intracellular Y5 RNA. a Schematic diagram of the procedure for mass spectrometric analysis of different samples. **b** i–iv MALDI-TOF spectra of HPA (i), mixture of CMP, UMP, AMP, and GMP (ii), RNase (iii), RNase-treated Syn-Y5 (iv). v Orbitrap Eclipse Tribrid spectrum of RNase-treated intracellular Y5 RNA from HeLa cells. **c** i MALDI-TOF spectrum of intracellular Y5 RNA from Ac_4ManNAz. ii Orbitrap Eclipse Tribrid spectrum of intracellular Y5 RNA from Ac_4GlcNAc labelled HeLa cells after treated with RNase. **d** MALDI-TOF spectra of (i) GlcNAcase, (ii) O-Glycosidase and (iii) PNGase F treated intracellular Y5 RNA from HeLa cells after RNase digestion. The spectra of (**b** v) and (**c** ii) were specially produced on a high-resolution Orbitrap Eclipse Tribrid mass spectrometer coupled with an EASY-nLC 1200 system in order to precisely reveal the variation of m/z peaks.

potential spatial hindrance of aptamer and the lack of other fast and efficient labelling method to the monosaccharide GlcNAc, here we referred these methods and developed the GlcISH-PLA by replacing the corresponding recognition components targeting to Y5 RNA and the metabolically labelled GlcNAz (Supplementary Fig. 48). The Probe-A-Y5 contained a sequence complementary to the part of Y5 RNA at 3′ end and another sequence complementary to parts of Circle-1 and Circle-2 probes at 5′ end. The Probe-B also contained a sequence complementary to parts of Circle-1 and Circle-2 probes at 3′ end and a DBCO at 5′ end. After delivered into the Ac_4GlcNAz metabolically labeled cells, the recognition of Probe-A-Y5 and Probe-B on GlcNAc-Y5 RNA brought them into close proximity, which further facilitated the closed loop of Circle-1 and Circle-2 by DNA ligase[61,62]. Subsequently, the rolling circle amplification (RCA) initiated from Probe-B produced a long single-stranded DNA amplicon[63], which could bind massive fluorophore-labelled detection probes (FDPs) for quantitively imaging with single-cell and single-molecule resolution owing to the one-target-one amplicon amplification process[64].

The feasibility of GlcISH-PLA was firstly demonstrated by in vitro PAGE analysis (Supplementary Fig. 49). After subjecting the GlcNAc-Y5 RNA collected from Ac_4GlcNAz-treated HeLa cells to the ISH-PLA procedure, the product exhibited a heavy accumulation in the loading well of the gel (Lane 2 in Supplementary Fig. 49), while the ISH-PLA mixture without Probe-B only exhibited bands of the raw compounds (Lane 3 in Supplementary Fig. 49), demonstrating the feasibility of GlcISH-PLA for GlcNAc-Y5 RNA.

https://doi.org/10.1038/s41467-026-72909-4

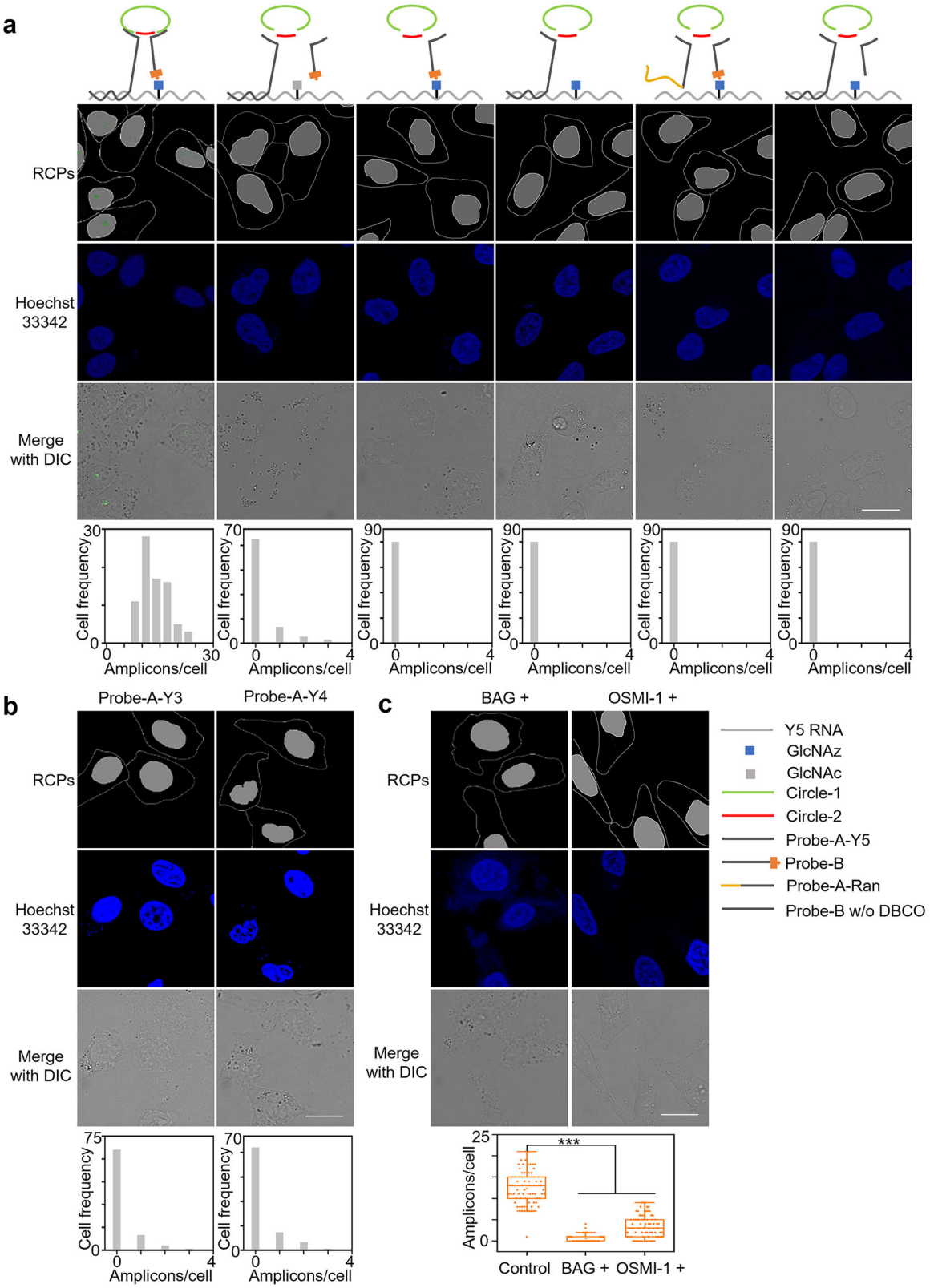

Next, we performed the GlcISH-PLA to HeLa cells (Fig. 7a, Column 1). To further demonstrated the specificity of GlcISH-PLA, cells without metabolic labeling (Column 2), GlcISH-PLA without Probe-A-Y5 (Column 3), without Probe-B (Column 4), replacing Probe-A-Y5 with Probe-A-Ran (Column 5), removing DBCO in Probe-B (Column 6), were set as control groups, respectively. To improve the resolution of images for quantification of the fluorescence dots, the cells after GlcISH-PLA procedure were subjected to CLSM imaging under STED mode, which reduced the overall fluorescence intensity but significantly improved the resolution for quantification. As a result, the Ac_4GlcNAz-treated cells after the normal GlcISH-PLA procedure exhibited obvious fluorescence dots inside cells, which was calculated to be 12.26 amplicons

Fig. 7 | In situ quantification of GlcNAc-Y5 RNA by GlcISH-PLA. a STED super-resolution images of GlcNAc-Y5 RNA visualized by GlcISH-PLA in HeLa cells. In RCA amplicons (RCPs) channels, the bright green dots represent GlcNAc-Y5 RNA amplicons, and cell nucleus are shown in gray (Hoechst 33342), and the outlines of cells are marked by a gray dashed line. Frequency histograms of the number of intracellular GlcNAc-Y5 RNA molecules per cell are presented on the bottom (cell number = 80). Scale bar: 20 μm. **b** STED super-resolution images of Y3 RNA or Y4 RNA visualized by GlcISH-PLA in HeLa cells. Frequency histograms of the number of intracellular GlcNAc on Y3 RNA or Y4 RNA per cell are presented on the bottom (cell number = 80). Scale bar: 20 μm. **c** STED super-resolution images of GlcNAc-Y5 RNA visualized by GlcISH-PLA in HeLa cells metabolically labeled with Ac_4GlcNAz and treated with 1.5 mM BAG or 20 μM of OSMI-1 at 37 °C for 48 h. Quantification of the average expression of intracellular GlcNAc-Y5 RNA molecules per cell is presented at the bottom (cell number = 80). Scale bar: 20 μm. In the box plots, the centre line represents the median, the box bounds indicate the first and third quartiles, and the whiskers extend to the minimum and maximum values. Statistical analysis was performed by unpaired two-tailed *t*-tests (*$p < 0.05$; **$p < 0.005$; ***$p < 0.0005$; NS, not significant), $n = 80$. The exact *p*-values are as follows: Control *vs* BAG +, $p = 7.08 \times 10^{-42}$; Control *vs* OSMI-1 +, $p = 2.14 \times 10^{-34}$.

per cell by ImageJ software collecting from 80 cells. In contrast, no fluorescence dot was found in any other control groups, and amplicons in these groups were all zero, which further demonstrated the reliability of GlcISH-PLA. By replacing the Probe-A-Y5 to Probe-A-Y3 or Probe-A-Y4 and performing the normal GlcISH-PLA procedure, tiny fluorescence dots were observed in the Ac_4GlcNAz-treated cells, which was calculated to be 0.23 amplicons per cell for Y3 RNA and 0.3 amplicons per cell for Y4 RNA (Fig. 7b). These results were agreed with the FRET imaging results that GlcNAc was not presented in Y3 and Y4 RNAs (Fig. 5).

To exclude the possible unspecific RCA amplicon generated from the Y5 RNA adjacent GlcNAc-modified proteins, the Ac_4GlcNAz metabolically labelled HeLa cells after cell fixation and permeabilization were treated with Pro. K to digest the proteins inside cells by degrading the serine amino acid linkages[12]. To investigate the structure influence of Pro. K incubation to living cells, the HeLa cells incubated with different concentrations of Pro. K and then subjected to 3-(4,5-dimethylthiazol2-yl)-2,5-diphenyltetrazolium bromide (MTT) assay, which maintained healthy viabilities above 95% (Supplementary Fig. 50a) and well-preserved morphology with normal cellular architecture (Supplementary Fig. 50b), demonstrating the negligible cell viability and structure influence of Pro. K incubation. After subjected to GlcISH-PLA, the Pro. K-treated cells exhibited obvious fluorescence dots with an average of 12.05 amplicons per cell (Supplementary Fig. 51), which was approximate to the value (12.26 amplicons per cell) of HeLa cells without Pro. K treatment, indicating that the GlcNAc-modified proteins cannot generate unspecific RCA amplicons.

To further validate the quantification results, the O-GlcNAc transferase (OGT) inhibitor benzyl-α-GalNAc (BAG)[65,66] and OSMI-1[67,68] was applied to inhibit the incorporation of GlcNAc into Y5 RNA, respectively. After performing the normal GlcISH-PLA procedure and STED super-resolution imaging, the amplicons in BAG and OSMI-1-treated HeLa cells decreased to 0.59 and 3.4 amplicons per cell (Fig. 7c), respectively. The GlcISH-PLA and STED super-resolution imaging was also performed on HaCaT, MCF-7 and MCF-10A cells (Supplementary Fig. 52), which exhibited 19.54, 11.55 and 15.43 amplicons per cell and decreased to 0.69, 1.41 and 1.89 amplicons per cell after BAG treatment and 3.83, 4.12 and 4.09 amplicons per cell after OSMI-1 treatment, respectively (Supplementary Fig. 52), indicating that the modification of GlcNAc to Y5 RNA very likely followed the conventional OGT-related approaches.

The levels of GlcNAc-Y5 RNA in these four cell lines were in good agreements with the E_{FRET} values in the FRET imaging results (Supplementary Fig. 53), demonstrating the reality of the GlcISH-PLA. Thus, the levels of intracellular GlcNAc-Y5 RNA could be successfully quantified by the developed GlcISH-PLA through STED super-resolution imaging.

Discussion

The glycoRNAs is an exciting and attractive finding in the field of glycobiology during recent years[12]. The existence of glycoRNAs has been demonstrated on cell surface[26–29] and exosomes[32,33]. Nevertheless, the existence of other types of glycoRNAs, particularly intracellular glycosylated RNA, still remains mysterious.

Here, we extend our perspective from N-glycans to GlcNAc modification. We design a general paradigm, which utilize a FRET strategy to preliminarily explore the potential GlcNAc-modified glycoRNAs inside mammalian cells with Y5 RNA as a model of the target glycoRNA. Through completely excising the glycoRNAs on cell surface with RNase treatment to exclude the interference of cell surface glycoRNAs, DBCO-Cy3 and FAM-DNA complementary to the sequence of Y5 RNA are delivered into the cells through cell permeabilization. The specificity of FRET signal is demonstrated by knocking out of Y5 RNA (Supplementary Fig. 5), inhibition of GlcNAc (Supplementary Fig. 5), and exclusion of the influence of RNA-binding proteins (Supplementary Fig. 6). The FRET signal from FAM to Cy3 in Ac_4GlcNAz labelled HeLa, HaCaT, MCF-7 and MCF-10A cells (Fig. 1b and Supplementary Figs. 8–10) provides the evidence of intracellular GlcNAc-Y5 RNA, and the tiny Cy3 fluorescence and negligible FRET signal in Ac_4ManNAz labelled cells implies the absence of Sia on intracellular Y5 RNA. Interestingly, the FRET signal in Ac_4GlcNAz labelled cells depends on the position of FAM on FAM-DNA probe (Fig. 1c and Supplementary Fig. 7), which provides an efficient method for the evaluation of GlcNAc modification site.

The distribution of GlcNAc-Y5 RNA inside these cells can be analyzed with the FRET signal from colocalization images. Compared to ER-Red and Golgi-Red stained cells, Hoechst 33342 stained cells show the highest colocalization coefficient (Fig. 2b–d and Supplementary Figs. 12–17), which demonstrated the main distribution of GlcNAc-Y5 RNA inside nucleus, consistent with the main distribution Y5 RNA reported previously[45], indicating a potential glycosylation pathway from the nucleus to cell surface.

We then design a target-specific approach to extract the intracellular Y5 RNA for demonstrating the existence of GlcNAc-Y5 RNA with PAGE analysis (Fig. 3a). This approach can be performed by extracting the total RNAs from the metabolically labelled or unlabelled and then RNase treated cells, and then capturing the Y5 RNA from obtained total RNAs with MB-Cap-Y5, which is subsequently released from the MBs with competitive displacement of DNA probe. The captured Y5 RNA from the metabolically labelled cells shows FAM fluorescence upon incubation with DBCO-FAM (Fig. 3e), verifying the presence of GlcNAc on Y5 RNA, which can further be demonstrated by CLSM imaging of glycosidase-treated cells and PAGE analysis of glycosidases incubated Y5 RNA samples.

After the permeabilized cells are treated with different glycosidases, only the GlcNAcase-treated cells showed great decrease of the FRET signal (Fig. 4b-e and Supplementary Figs. 24, 26-31). Meanwhile, the GlcNAcase incubated Y5 RNA samples exhibit efficient degradation of GlcNAc monosaccharide (Fig. 4f, g). These results validate the GlcNAc monosaccharide modification of Y5 RNA inside cells. Moreover, the GlcNAc monosaccharide modification of Y5 RNA possesses universality in different cells (Supplementary Fig. 32), but other Y RNAs, such as Y3 and Y4 RNAs do not give positive evidence to support the presence of GlcNAc (Fig. 5 and Supplementary Figs. 33 and 34), indicating that the GlcNAc modification of Y RNAs

was not a common existence. Nonetheless, the RNA sequencing of the intracellular GlcNAc-modified total RNAs indicates that many other RNAs, including tRNA-derived small RNAs, snoRNAs, piRNA clusters, and specific microRNAs were modified with GlcNAc (Supplementary Fig. 36), and they can be sensitively imaged by the FRET imaging even with low expression and GlcNAcylation levels (Supplementary Fig. 37).

Since the Y5 RNA is modified by the GlcNAc monosaccharide and its sequence is well known, the components of GlcNAc on intracellular Y5 RNA can be investigated with mass spectrometric analysis (Fig. 6a). Nevertheless, we fail to directly acquire a complete molecular ion peak of the collected intracellular Y5 RNA due to the low ionization efficiency. As an alternative way, we firstly degraded the Y5 RNA by RNase and/or glycosidases digestion. Using syn-Y5 as control, the Y5 RNA samples collected from all four cell lines show an extra peak around m/z of 537.48, which shifts to m/z around 578.48 after the cells are firstly metabolically labelled with Ac_4GlcNAc by the Orbitrap Eclipse Tribrid mass spectrometer (Fig. 6b, c and Supplementary Figs. 39 and 40). Besides, this extra peak disappears upon GlcNAcase treatment (Fig. 6d and Supplementary Fig. 42). These results demonstrate that it is associated with the conjugate of GlcNAc and ribonucleotides.

The components of the conjugate are further investigated with MALDI-TOF MS/MS analysis of the peak at m/z around 537.5, which shows a new peak at m/z around 396.4 for all the four cell lines (Supplementary Fig. 45). Upon expanding the detection range using the Orbitrap Eclipse Tribrid mass spectrometer, peaks around m/z of 1075.96 ($[M\text{-}H]^-$) were simultaneously observed (Supplementary Fig. 46), which was twice of the peaks around m/z of 537.48 after plus one hydrogen mass. Combining with the isotopic peaks (Supplementary Fig. 47), it can be deduced that the conjugate of GlcNAc and ribonucleotides can exhibit singly charged and loss of two hydrion versions in MS analysis.

The levels of GlcNAc-Y5 RNA inside different cell lines are quantified with the developed GlcISH-PLA procedure, which exhibits certain feasibility and reliability (Supplementary Fig. 49 and Fig. 7a). After the number of the bright pixels in the STED super-resolution images was counted and analyzed by ImageJ software, the GlcNAc-Y5 RNA levels in HeLa, HaCaT, MCF-7 and MCF-10A cells are calculated to be 12.26, 19.54, 11.55 and 15.43 amplicons per cell, which remains unchanged in the Pro. K treated cells (Supplementary Fig. 51), but obviously decrease in the GlcNAcylation inhibitors treated cells (Fig. 7c and Supplementary Fig. 52), demonstrating the reality of the quantitative results.

In sum, we designed a general paradigm for studying glycoRNA from multiple perspectives and discovered that the intracellular Y5 RNA was modified with GlcNAc monosaccharide, which was mainly distributed in nucleus. The components of intracellular glycosylated Y5 RNA in four different cells were demonstrated by the specially designed procedures for fluorescence and FRET imaging, Y5 RNA extracting, and RNase and/or glycosidases digestion coupled with PAGE and MS or MS/MS analysis. Moreover, a GlcISH-PLA procedure was developed to in situ quantify the levels of intracellular glycoRNAs with single-cell and single-molecule resolution. These findings innovate the distribution and quantitation information of glycoRNAs, which will greatly promote the functional research of glycoRNAs.

Methods

DNA sequences (5′-3′)

All DNA with following sequences were customized from Sangon Biological Engineering Technology & Co., Ltd. (Shanghai, China):

Com-Y5-1: AAAACAGCAAGCTAGTCAAGCGCGGTTGTGGGGGGAGACAATGTTAAAT
/i6FAMdT/CAACTT AACAATAACCCACAACACTCGGACCAACT

Com-Y5-2: AAAACAGCAAGCTAGTCAAGCGCGGTTGT/i6FAMdT/GGGGGGAGACAATGTT
AAATCAACTT AACAATAACCCACAACACTCGGACCAACT

Com-Y5-3: AAAACAGCAAGCTAGTCAAGCGCGGTTGTGGGGGGAGACAATGTTAAAT
CAACTTAACAATAACCCACAACACTCGGACCAAC/i6FAMdT/

Com-Y5-4: AAAACAGCAAGCTAGTCAAGCGCGGTTGTGGGGGGAGACAATGTTAAAT
CAACTTAACAATAACCCACAACACT/i6FAMdT/CGGACCAACT

Com-Y5-5: AAAACAGCAAGCTAGTCAAGCGCGGTTGTGGGGGGAGACAATGTTAAAT
CAACTT/i6FAMdT/AACAATAACCCACAACACTCGGACCAACT

Com-Y5-6: AAAACAGCAAGCTAGTCAAGCGCGGTTGTGGGGGGAGACAAT/i6FAMdT/GTT
AAATCAACTTAACAATAACCCACAACACTCGGACCAACT

Com-Y5-7: AAAACAGCAAGCTAGT/i6FAMdT/CAAGCGCGGTTGTGGGGGGAGACAATGTT
AAATCAACTTAACAATAACCCACAACACTCGGACCAACT

Com-Y5-8: FAM-AAAACAGCAAGCTAGTCAAGCGCGGTTGTGGGGGGAGA-CAATGTTAAA
TCAACTT AACAATAACCCACAACACTCGGACCAACT

Com-miR-140-3p: CTACCATAGGGT/i6FAMdT/AAAACCACTG

T84: TTTTTTTTTTTTTTTTTTTTTTTTTTTTTTTTTTTTT/i6FAMdT/TTTTTTTTTTTTTTTTT
TTTTTTTTTTTTTTTTTTTTTTTTTT

Syn-Y5: AGUUGGUCCGAGUGUUGUGGGUUAUUGUUAAGUU-GAUUUAACAUUGUCUCCC
CCCACAACCGCGCUUGACUAGCUUGCUGUUUU

Cap-Y5: Biotin-TTTTTTTTTTAAAACAGCAAGCTAGTCAAGCGCGGTTGTGGT-GAATGAATA
GTTGAGCGC

Rel-Y5: GCGCTCAACTATTCATTCACCA-CAACCGCGCTTGACTAGCTTGCTGTTTT

Cap-Y3: Biotin-TTTTTTTTTTAAAAGGCTAGTCAAGTGAAGCAGTGGGAGTGT-GAATGAATA
GTTGAGCGC

Rel-Y3: GCGCTCAACTATTCATTCA-CACTCCCACTGCTTCACTTGACTAGCCTTTT

Cap-Y4: Biotin-TTTTTTTTTTAAAAAGCCAGTCAAATTTAGCAGTGGGGGGGT-GAATGAATA
GTTGAGCGC

Rel-Y4: GCGCTCAACTATTCATTCACCCCCCCACTGCTAAATTT-GACTGGCTTTTT

Cap-R1: Biotin-TTTTTTTTTTGCCGAAGCACTCCAAAAAAAGGGCC-GACTGGTTGCCGGTT
TGTATATCAG

Rel-R1: CTGATATA-CAAACCGGCAACCAGTCGGCCCTTTTTTTGGAGTGCTTCGGC

Com-Y3-1: AAAAGGCTAGTCAAGTGAAGCAGTGGGAGTGGA-GAAGGAACAAAGAAAT
/i6FAMdT/CTGTAACTGGTTGTGATCAATTAGTTGTAAACACCACTGCACTCGGA
CCAGCC

Com-Y4-1: AAAAAGCCAGTCAAATTTAGCAGTGGGGGGTTGTA-TACCAACTTTAGTGACAC
T/i6FAMdT/AA
TGTTAATAAGTTCTGATAACCCACTACCATCGGACCAGCC

Y5 DNA-1: AGTTGGTCCGAGTGTTGTGGGTTAT/iCy3/TGTTAAGTTGATTTAACATTGTCTC
CCCCCACAA CCGCGCTTGACTAGCTTGCTGTTTT

Y5 DNA-2: AGTTGGTCCGAGTGTTGTGGGTTATTGTTAAGTT-GAT/iCy3/TTAACATTGTCTC

CCCCCACAA CCGCGCTTGACTAGCTTGCTGTTTT

Y5 DNA-3: AGTTGGTCCGAGTGTTGTGGGTTATTGTTAAGTT-GATTTAACAT/iCy3/TGTCTC

CCCCCACAA CCGCGCTTGACTAGCTTGCTGTTTT

Probe-A-Y5: GGA TAA AGG ATT GGA TTT ATG AAT TTA ACA TTG TCT CGG GGG TGT TGG

CGC GAA CTG AT

Probe-B: DBCO-AAA AAA AAA AGC AAT GAC GGT GTC AGA GTA AC

Circle-1: P-ATC CTT TAT CCC AGT GAA TGC GAG TCT CGA GGT GCA TTC ATA TCA GCA

GCC GTC GTT ACT CTG AC

Circle-2: P-ACC GTC ATT GCT TTTCA TAA ATC CA

FDP: Alexa488-AACT ATA CAA CAT AC TAC CTC A

Probe-A-Ran: GGA TAA AGG ATT GGA TTT ATG AAT TTA ACA TTG TCT CAA AAA AAA

AAA AAA AAA AAA AA

Probe-A-Y3: GGA TAA AGG ATT GGA TTT ATG AAT TTA ACA TTG TCT CCA CCA CTG CAC

TCG GAC CAG CC

Probe-A-Y4: GGA TAA AGG ATT GGA TTT ATG AAT TTA ACA TTG TCT CAC CCA CTA CCA

TCG GAC CAG CC

Cell culture

HeLa and HaCaT cells were cultured in DMEM. MCF-7 and MCF-10A cells were cultured in RPMI-1640. All the media contained 10% FBS (Gibco), penicillin (100 μg/mL) and streptomycin (100 μg/mL), and all the cells were cultured at 37 °C under a humidified 5% CO_2 atmosphere.

Cell metabolism

40 mM of stocks of Ac_4GlcNAc and Ac_4ManNAz were prepared in DMSO. The metabolic labelling experiments were performed by incubating the cells in DMEM or RPMI-1640 containing 40 μM of Ac_4GlcNAc or Ac_4ManNAz at 37 °C under a humidified 5% CO_2 atmosphere for 48 h.

Excising of RNA on cell membrane

Cells were firstly seeded on 4-well confocal dishes and cultured overnight. After washing with PBS, the cells were treated with 100 μL PBS (pH 7.5) containing 0.4% BSA, 0.4 mg/mL RNase A, 1000 U/mL RNase T1, 2 mM Tris-HCl, 60 mM NaCl and 1 mM EDTA at 37 °C for 1 h. The cells without RNase treatment were used as negative controls. After blocked with PBS (pH 7.5) containing 0.5% BSA on ice for 30 min, the cells were incubated with 100 μL PBS (pH 7.5) containing 0.5% BSA and 40 μg/mL J2 for 30 min on ice, and then stained with 80 μg/mL Goat Anti-Mouse lgG AF 488 antibody in 100 μL PBS (pH 7.5) containing 0.5% BSA for 30 min on ice in the dark. After the cells were carefully washed with PBS (pH 7.5) containing 0.5% BSA for three times, the fluorescence of the cells was collected by CLSM imaging from 500 to 570 nm at the excitation wavelength of 488 nm with Leica Application Suite X.

CRISPR/Cas9 knockout of Y5 RNA

Dual-guide CRISPR vectors were designed to disrupt the target gene, with each construct expressing two sgRNAs under H1 and U6 promoters alongside Cas9 and selection markers. Specifically: Vector 1: H1-sgRNA1 (5′-TTTCCTGGATCATTGACCCG-3′)–U6-sgRNA2 (5′-TGTCAACTCTAAGCAACTGC-3′)–EF1α-Cas9–CMV-Puro. Vector 2: H1-sgRNA3 (5′-GCGTGCCTGTGGCTGAAGCG-3′)–U6-sgRNA4 (5′-CTAA-GAATGGAGGTGTTCAT-3′)–EF1α-Cas9–CMV-Puro. HeLa cells were co-transfected with both vectors using Lipofectamine 3000. After 48 h incubation, the transfected cells were selected with 2 μg/mL puromycin for 7 days, followed by FACS sorting of EGFP+ populations to enrich doubly transfected cells.

FRET imaging

Cells were firstly seeded on 4-well confocal dishes and cultured overnight. After washing with PBS, the cells were metabolically labelled with Ac_4GlcNAc or Ac_4ManNAz, and treated with 100 μL PBS (pH 7.5) containing 0.4% BSA, 0.4 mg/mL RNase A, 1000 U/mL RNase T1, 2 mM Tris-HCl, 60 mM NaCl and 1 mM EDTA at 37 °C for 1 h. After fixed with 4% paraformaldehyde at 37 °C for 15 min, the cells were dealt with 0.25% Triton X-100 at 37 °C for 10 min to perforate cell membrane, and then stained with DBCO-Cy3 (10 μM in PBS) at 4 °C for 1 h. Afterward, the cells were incubated with Com-DNAs (10 μM in PBS) at 37 °C for 1 h. The cells without metabolically labelling were used as negative controls. After carefully washed with PBS for three times, the resulting cells were subjected to CLSM imaging and analyzed by Leica Application Suite X. The FAM channel was collected from 500 to 550 nm with an excitation wavelength of 488 nm. The Cy3 channel was collected from 550 to 600 nm with an excitation wavelength of 520 nm. The FRET channel was collected from 550 to 600 nm with an excitation wavelength of 488 nm. To demonstrate the specificity of FRET imaging, the cells were pre-treated with CRISPR/Cas9 knockout of Y5 RNA or 25 μM DON at 37 °C for 48 h and then subjected to the same FRET imaging procedure.

The AntiRo60-Cy3 was prepared by gradually adding 12.6 μL of 10 mg/mL Cy3 NHS ester to 1 mL of 10 mg/mL AntiRo60 under gently swirling. The reaction tube was placed in a dark environment and incubated at room temperature for 60 min, and then dialyzed overnight using dialysis bag to remove excess Cy3 NHS ester and obtain AntiRo60-Cy3.

To investigate the possible false-positive FRET between GlcNAc and Ro60 or any potential RNA-binding proteins, the HeLa cells were firstly seeded on 4-well confocal dishes and cultured overnight. After washing with PBS, the cells were treated with 100 μL PBS (pH 7.5) containing 0.4% BSA, 0.4 mg/mL RNase A, 1000 U/mL RNase T1, 2 mM Tris-HCl, 60 mM NaCl and 1 mM EDTA at 37 °C for 1 h. After fixed with 4% paraformaldehyde at 37 °C for 15 min, dealt with 0.25% Triton X-100 at 37 °C for 10 min to perforate cell membrane, and then incubated with Com-Y5-1 (10 μM in PBS) at 37 °C for 1 h. Afterward, the cells were incubated with 100 μL 500 μg/mL AntiRo60-Cy3 or 50 μM NHS-Cy3 for 1 h at 37 °C. After carefully washed with PBS for three times, the resulting cells were subjected to CLSM imaging and analyzed by Leica Application Suite X.

Ro60-Cy3 extraction

The HeLa cells were incubated with 50 μM NHS-Cy3 for 1 h at 37 °C and then lysed in NP-40 buffer (50 mM Tris-HCl pH 7.4, 150 mM NaCl, 1% NP-40) supplemented with protease/phosphatase inhibitors. Lysates were pre-cleared with protein A/G beads for 1 h at 4 °C to reduce non-specific binding. Subsequently, supernatants were incubated overnight at 4 °C with 2 μg of AntiRo60 pre-bound to magnetic beads, followed by three washes with high-stringency buffer (500 mM NaCl, 0.1% Tween-20). Ro60-Cy3 was eluted using low-pH glycine (0.1 M, pH 2.5) or Laemmli buffer for downstream analysis.

SDS-PAGE analysis

Ro60-Cy3 protein samples were denatured in Laemmli sample buffer (62.5 mM Tris-HCl pH 6.8, 2% SDS, 10% glycerol, 0.01% bromophenol blue) containing 100 mM DTT at 95 °C for 5 min, which were then separated on 12% resolving/4% stacking polyacrylamide gels cast in Tris-glycine buffer systems, with electrophoresis performed initially at 80 V through the stacking gel followed by 120 V in the resolving gel until the dye front reached the bottom. Gels were subsequently fixed in 40% methanol/10% acetic acid (v/v) for 30 min, stained with 0.1% Coomassie Brilliant Blue R-250 for 1 h, and detained in methanol/acetic acid solution until clear for visual detection by PowerPac™ basic electrophoresis analyzer.

Colocalization analysis

After the cells were treated with the same procedure as FRET imaging, the cells were treated with 10 μg/mL of Hoechst 33342 in Hanks for 10 min at room temperature, washed with PBS, and subjected to CLSM imaging for nucleus colocalization analysis. For ER colocalization analysis, the cells were treated with 500 nM of ER-Red in Hanks for 20 min at 37 °C, washed with PBS, and then subjected to CLSM imaging. For Golgi colocalization analysis, the cells were sequentially treated with Golgi-Red in Hanks at 1:100 dilution for 30 min at 4 °C, and DMEM or RPMI-1640 at 37 °C for 30 min.

Total RNA extraction

After Trizol reagent was mixed with the cells for few seconds, the mixture was incubated at room temperature for 5 min, added with 0.2 × volume of 100% chloroform to totally rotate at room temperature for 3 min, and followed with centrifugation at 13,900 × *g* for 15 min at 4 °C. The aqueous phase was carefully transferred to a fresh tube and mixed with equal volume of isopropyl alcohol. The resulting mixture was incubated at room temperature for 10 min. After short vortex and centrifugation at 13,900 × *g* for 15 min at 4 °C, the precipitate was collected and added with 1 × volume of 75% ethanol to remove excess isopropyl alcohol, which was shortly rotated, centrifugalized at 7820 × *g* for 5 min at 4 °C twice, and naturally dried. The obtained total RNA was dissolved in DEPC-treated water for storage.

Collection of Y RNAs by MB separation

The MBs were firstly washed with Buffer I (10 mM pH 7.5 Tris-HCl containing 1 mM EDTA, 1 M NaCl and 0.01% ~ 0.1% Tween-20) by vortex and magnetic separation twice. The washed MBs were incubated with Cap-Y5 (twice the amount of streptavidin) diluted in Buffer I at room temperature on a rotary mixer for 30 min. After washed twice with Buffer I, the obtained MB-Cap-Y5 was incubated with the total RNA in Buffer II (10 mM pH 7.5 Tris-HCl containing 20 mM $MgCl_2$) at 37 °C on a rotary mixer for 1 h. The resulting MB-Cap-Y5/Y5 RNA was collected by magnetic separation and washed with Buffer II twice.

The successful capture of Y5 RNA on MB-Cap-Y5 was demonstrated with Y5 RNA extracted from 4 kinds of Ac_4GlcNAc metabolically labelled cells. After magnetic separation and washing, 100 μM of DBCO-FAM was added to the resulting MB-Cap-Y5/GlcNAc-Y5 RNA to incubate at 4 °C on a rotary mixer for 1 h. After magnetic separation, the MBs were washed with Buffer II twice and subjected to CLSM imaging in a confocal dish. The FAM channel of MB-Cap-Y5 was collected from 500 to 570 nm with an excitation wavelength of 488 nm.

To collect Y5 RNA, the MB-Cap-Y5/Y5 RNA was incubated with Rel-Y5 in Buffer II at 37 °C on a rotary mixer for 1 h. After magnetic separation, the supernatant containing the Y5 RNA was transferred to a new centrifuge tube. The concentration of Y5 RNA in the sample was quantified by Nanodrop One Micro UV−visible spectrophotometer. Y3 and Y4 RNA were collected with the same procedure by using Cap-Y3, Rel-Y3, Cap-Y4 and Rel-Y4, respectively.

Gel electrophoresis analysis

4 μL of nucleotide samples was respectively mixed with 1 μL of 6 × loading buffer and 1 μL of 6 × Ultra Power dye. The mixtures were loaded into 8% native polyacrylamide gel and run at 110 V for 60 min in 1 × TBE buffer. The obtained gel was imaged by Molecular Imager Gel Doc XR software.

The fluorescence analysis of gel electrophoresis was performed by incubating 4 μL of nucleotide samples with 1 μL 100 μM DBCO-FAM at 4 °C for 1 h, mixing the solution with 1 μL of 6 × loading buffer, and then loading the mixture into 8% native polyacrylamide gel to run at 110 V for 60 min in 1 × TBE buffer.

Enzyme treatments of different cells

After the cells were seeded on 4-well confocal dishes to perform metabolic labelling with Ac_4GlcNAz or Ac_4ManNAz, RNase treatment, PFA fixation, permeabilization treatment, DBCO-Cy3 incubation, and Com-Y5-1 recognition, they were incubated with 400 U/mL GlcNAcase at 37 °C for 1 h, 4000 kU/mL O-Glycosidase at 37 °C for 3 h or 25 kU/mL PNGase F at 37 °C for 1 h for GlcNAcase, O-glycosidase or PNGase F digestion of Y5 RNA.

Enzyme digestion of Y5 RNA

GlcNAcase digestion of Y5 RNA was performed by adding 1 μL of GlcNAcase and 1 μL of GlyoBuffer 1 (10×) in 9 μL of Y5 RNA sample (10 μg/mL) to incubate at 37 °C for 1 h. O-Glycosidase digestion of Y5 RNA was performed by mixing 7 μL of Glycoprotein Denaturing Buffer (10×) with 3 μL of Y5 RNA sample (10 μg/mL) to incubate at 37 °C for 30 min, and then adding 2 μL of GlycoBuffer 2 (10×), 2 μL of 10% NP-40, 4 μL of O-Glycosidase and 2 μL DEPC water in the mixture to incubate at 37 °C for 3 h. PNGase F digestion of Y5 RNA was performed by mixing 3 μL of Y5 RNA sample (10 μg/mL) with 7 μL of Glycoprotein Denaturing Buffer (10×) at 100 °C for 10 min, and then adding 2 μL of GlycoBuffer 2 (10×), 2 μL of 10% NP-40, 1 μL of PNGase F and 6 μL DEPC water in the mixture to incubate at 37 °C for 1 h. Protease-K digestion of Y5 RNA was performed by adding 5 μL of Protease-K (10 μg/mL) into 5 μL of Y5 RNA sample (10 μg/mL) and then incubated at 37 °C for 1 h.

RNase digestion of Y5 RNA was performed by mixing Y5 RNA sample with the mixture of 0.4 mg/mL RNase A and 1000 U/mL RNase T1 at equal volume to incubate at 37 °C for 1 h. The inhibition to RNase digestion was performed by adding 4000 U/mL RNase inhibitor in RNase mixture to incubate at 37 °C for 1 h.

RNA sequencing

Total RNAs from the Ac_4GlcNAz metabolically labelled and then RNase-treated HeLa cells were extracted with a traditional procedure using Trizol reagent. The azide-containing RNAs (50 μg) was digested with Pro. K for 45 min. Following digestion, the sample was incubated with click reaction reagents containing alkyne-biotin at 55 °C for 20 min. The resulting RNA was purified, and 200 ng aliquot was reserved as the input control. Streptavidin-modified magnetic beads were blocked at 25 °C for 1 h and subsequently washed twice. The purified RNA from the click reaction was then incubated with the blocked streptavidin-modified beads for 2 h at 4 °C with rotation. Post-incubation, the bead-bound complexes were subjected to sequential washes. Bound RNA was eluted from the beads using streptavidin elution buffer during 10 min reaction to yield the immunoprecipitated sample. Both the input and immunoprecipitated RNA samples were then processed for PANDORA-seq library construction and sequencing. The sncRNA annotation was performed using the SPORTS1.1 software package.

MALDI-TOF mass spectrometer analysis

MALDI-TOF mass spectrometric experiments were performed on a MALDI-7090 mass spectrometer (Shimadzu, Japan) with a 355 nm Nd:YAG laser, a repetition rate of 200 Hz, and an acceleration voltage of 20 kV. The MALDI-MS spectra were acquired using the negative linear mode with a 100 μm diameter laser beam. For each spectrum, 200 profiles (20 shots to accumulate 1 profile) from different positions of the target spot (automatic mode) were collected. For GlcNAc-Y5 RNA analysis, the RNA samples were treated with RNase at 37 °C for over 3 h, and then 1.5 μL of the mixture and 1.5 μL of 20 mg mL^{-1} HPA dissolved in 50 mM disodium citrate solution of 9:1 acetonitrile and water (v/v) as matrix were successively spotted on a 384-well stainless steel MALDI plate, and left to dry.

Higher-resolution Orbitrap Eclipse Tribrid mass spectrometer analysis

Experiments were performed on an EASY-nLC 1200 system coupled with an Orbitrap Eclipse Tribrid mass spectrometer (ThermoFisher Scientific, USA) as further specified in respective experiments. The digested nucleosides were resuspended in MS buffer A (LC-MS water with 0.1% Formic Acid (FA)) at 0.5 mg/mL, and loaded on an in-house packed C18 column (25 cm, 2.6 μm Accucore (Thermo Fisher Scientific), 100 μm i.d.). Separation was carried out at a constant flow rate of 40 mL/min using MS buffer A and buffer B (ACN with 0.1% FA (v/v). The gradient was referred from the previous protocol. Specifically, 0–2 min, 0% B; 2–20 min, 0–16% B; 20–40 min, 16–72% B; 40–42 min, 72–100% B; 42–52 min, 100% B; 52–54 min, 100–0% B; 54–65 min, 0% B. The injection volume was 5 μL. The Orbitrap Eclipse Tribrid mass spectrometer was operated in negative ionization mode for canonical nucleotides (R = 120k; AGQ target = 400,000; MaxIT = 100 ms; RF Lens = 60%; mass range = 200–1500; centroid data).

Cell viability assay

To assess the cell viability influence of Pro. K, the cells were cultured in 96-well plates at a density of 5×10^4 cells/mL and incubated for 24 h. Subsequently, the cells were treated with varying concentrations of Pro. K, and co-incubated for an additional 24 h. Thereafter, 10 μL of MTT (3-(4,5-dimethylthiazol2-yl)-2,5-diphenyltetrazolium bromide) stock solution (5.0 mg/mL) in PBS was added to each well. Following a 4 h incubation, the medium was removed, and the resulting MTT-formazan crystals in each well were dissolved in 100 μL of DMSO. The plates were shaken for 1 min, and the absorbance was measured at 562 nm using a microplate reader (Cmax Plus, Molecular Devices, Shanghai).

In vitro GlcISH-PLA procedure

1 μL of Y5 RNA (100 nM) collected from Ac_4GlcNAz labelled HeLa cells was mixed with 1 μL of Probe-A (1 μM), 1 μL of Probe-B (1 μM), 1 μL of Circle-1 (1 μM), 1 μL of Circle-2 (1 μM) and 5 μL of PBS. After incubated at 37 °C for 2 h, the mixture was added with 2 μL of T4 DNA ligase (5 U in T4 ligation buffer, containing 40 mM Tris-HCl, 10 mM DTT, 10 mM $MgCl_2$ and 0.5 mM ATP (pH 7.8)) and 8 μL of H_2O. After incubated at 25 °C for 2 h, the mixture was further added with 0.25 μL of phi29 DNA polymerase, 3 μL of dNTPs (containing 10 mM of dATP, dCTP, dGTP, and dTTP), 3 μL of phi29 buffer (10×, containing including 20 mM Tris-HCl, 50 mM KCl, 10 mM $(NH_4)_2SO_4$, 2 mM $MgSO_4$, 0.1% Tween-20 (pH 8.8)) and 3.25 μL of H_2O. After incubated at 37 °C for 2 h, the reaction solution was placed in 65 °C water bath pot for 10 min to stop the reaction and subjected to PAGE analysis.

GlcISH-PLA procedure on cells

Cells were firstly seeded on 4-well confocal dishes and cultured overnight. After washing with PBS, the cells were metabolically labelled with Ac_4GlcNAc at 37 °C for 48 h. To inhibit the GlcNAcylation, the cells were treated with extra 1.5 mM of BAG or 20 μM of OMSI-1 simultaneously. After fixed with 4% paraformaldehyde at 37 °C for 15 min, the cells were dealt with 0.25% Triton X-100 at 37 °C for 6 min to perforate cell membrane. To digest intracellular proteins, the fixed and permeabilized cells were treated with 50 μg/mL Pro. K at 37 °C for 1 h. The cells were then treated with the mixture containing 10 μL of saline-sodium citrate buffer (SSC) buffer (20×), 2.5 μL of Probe-A (10 μM), 2.5 μL of Probe-B (10 μM), 2.5 μL of Circle-1 (10 μM), 2.5 μL of Circle-2 (10 μM), 5 μL of DTT (100 mM), 10 μL of yeast tRNA (10 mg/mL), 2.5 μL of RiboLock RNase inhibitor (40 U/μL) and 62.5 μL of RNase-free water at 37 °C overnight. After washing with PBS-T (PBS containing 0.05% Tween-20) for 3 times at room temperature to remove excess unhybridized oligonucleotide probes, the cells were incubated with the circularization reaction mixture contain 5 μL of of SSC (20×), 5 μL of ligase reaction buffer (10×), 1.25 μL of RiboLock RNase inhibitor (40 U/μL), 1.25 μL of T4 DNA ligase (40 U/μL) and 37.5 μL of RNase-free water at 37 °C for 2 h. After another wash with PBS-T, the cells were incubated with 50 μL of RCA mixture containing 1 μL of phi29 DNA polymerase, 5 μL of phi29 DNA polymerase reaction buffer (10×), 15 μL of dNTPs, 27.75 μL of RNase-free water, and 1.25 μL of 40 U/μL RiboLock RNase inhibitor at 37 °C for 2 h. After washing twice with PBS-T, the cells were incubated with the mixture containing 1 μL of FDP (100 nM), 10 μL of SSC (20×), 15 μL of formamide, 10 μL of salmon sperm DNA (10 ng/μL) and 64 μL of H_2O at 37 °C for 30 min to unfold and bind FDP. After carefully washed with PBS-T for three times, the cells were treated with 100 μL of Hoechst 33342 (10 μg/mL in Hanks buffer) for 10 min at room temperature. After washed with PBS-T, the cells were subjected to CLSM imaging under STED mode. The FAM channel was collected from 500 to 600 nm with an excitation wavelength of 488 nm.

Quantification and statistical analysis

The images in Fig. 2 and Supplementary Figs. 4 and 12–17 were acquired with a ×63 oil immersion objective to obtain the subcellular distribution of GlcNAc-Y5 RNA. The acquired fluorescence intensity of every cell in each frame was analyzed by using Leica Application Suite X (Leica, Germany), in which the fluorescence intensity profiles along the predetermined lines were obtained by the line drawing tool. The colocalization analyses of the data were conducted by Origin software. The relative fluorescence intensity was calculated by comparing the signal from each group to that of the group showing the highest signal. More than three biological replicates of each imaging group were performed, showing similar trends.

In Supplementary Figs. 23 and 25–30, the average fluorescence intensity of all cells in each frame was calculated by ImageJ (Version 1.52r). The fluorescence intensity of more than 10 cells per frame was collected for further statistical analysis. All the statistical calculations were performed with OriginPro 2023b. The number of bright pixels was counted by particle analysis in ImageJ to determine the copy number of amplicons per cell. Statistical significance was determined by *t*-test as not significant, $P < 0.05$ (*), $P < 0.005$ (**) and $P < 0.0005$ (***).

Reporting summary

Further information on research design is available in the Nature Portfolio Reporting Summary linked to this article.

Data availability

Mass spectrometry and quantitative data for Figs. 2b–d, 3d, e, 4c–g, 5b, c, 6b–d, 7 and Supplementary Figs. 4, 6, 11–17, 19–35, 38–40, 42–46, 49–53 are available in the Source data file. Source data are provided with this paper. The raw RNA sequencing dataset for Supplementary Fig. 36 is available on Gene Expression Omnibus under accession number GSE328403. The published article includes all the data analyzed during this study. Source data are provided with this paper.

References

1. Varki, A. Glycan-based interactions involving vertebrate sialic-acid-recognizing proteins. *Nature* **446**, 1023–1029 (2007).
2. Woods, R. J. Predicting the structures of glycans, glycoproteins, and their complexes. *Chem. Rev.* **118**, 8005–8024 (2018).
3. Ohtsubo, K. & Marth, J. D. Glycosylation in cellular mechanisms of health and disease. *Cell* **126**, 855–867 (2006).
4. Xiao, H., Woods, E. C., Vukojicic, P. & Bertozzi, C. R. Precision glycocalyx editing as a strategy for cancer immunotherapy. *Proc. Natl. Acad. Sci. USA* **113**, 10304–10309 (2016).
5. Reily, C., Stewart, T. J., Renfrow, M. B. & Novak, J. Glycosylation in health and disease. *Nat. Rev. Nephrol.* **15**, 346–366 (2019).
6. Yamakawa, N. et al. Systems glycomics of adult zebrafish identifies organ-specific sialylation and glycosylation patterns. *Nat. Commun.* **9**, 4647 (2018).

7. Boltje, T. J., Buskas, T. & Boons, G. J. Opportunities and challenges in synthetic oligosaccharide and glycoconjugate research. *Nat. Chem.* **1**, 611–622 (2009).
8. Paulson, J. C., Blixt, O. & Collins, B. E. Sweet spots in functional glycomics. *Nat. Chem. Biol.* **2**, 238–248 (2006).
9. Moremen, K. W., Tiemeyer, M. & Nairn, A. V. Vertebrate protein glycosylation: diversity, synthesis and function. *Nat. Rev. Mol. Cell Bio.* **13**, 448–462 (2012).
10. Hart, G. W., Housley, M. P. & Slawson, C. Cycling of O-linked β-N-acetylglucosamine on nucleocytoplasmic proteins. *Nature* **446**, 1017–1022 (2007).
11. Vocadlo, D. J., Hang, H. C., Kim, E. J., Hanover, J. A. & Bertozzi, C. R. A chemical approach for identifying O-GlcNAc-modified proteins in cells. *Proc. Natl. Acad. Sci. USA* **100**, 9116–9121 (2003).
12. Flynn, R. A. et al. Small RNAs are modified with N-glycans and displayed on the surface of living cells. *Cell* **184**, 3109–3124 (2021).
13. Shi, J., Zhou, T. & Chen, Q. Exploring the expanding universe of small RNAs. *Nat. Cell Biol.* **24**, 415–423 (2022).
14. Gross ßhans, H. & Filipowicz, W. Molecular biology: the expanding world of small RNAs. *Nature* **451**, 414–416 (2008).
15. Bartel, D. P. Metazoan MicroRNAs. *Cell* **173**, 20–51 (2018).
16. Schimmel, P. The emerging complexity of the tRNA world: mammalian tRNAs beyond protein synthesis. *Nat. Rev. Mol. Cell.Biol.* **19**, 45–58 (2018).
17. Shi, J. et al. PANDORA-seq expands the repertoire of regulatory small RNAs by overcoming RNA modifications. *Nat. Cell Biol.* **23**, 424–436 (2021).
18. Gu, W. et al. Peripheral blood non-canonical small non-coding RNAs as novel biomarkers in lung cancer. *Mol. Cancer* **19**, 159 (2020).
19. Wang, H. et al. CPA-seq reveals small ncRNAs with methylated nucleosides and diverse termini. *Cell Discov* **7**, 25 (2021).
20. Chen, C. J. & Heard, E. Small RNAs derived from structural non-coding RNAs. *Methods* **63**, 76–84 (2013).
21. Yue, T. et al. SLFN2 protection of tRNAs from stress-induced cleavage is essential for T cell-mediated immunity. *Science* **372**, 703 (2021).
22. Schorn, A. J., Gutbrod, M. J., LeBlanc, C. & Martienssen, R. LTR-retrotransposon control by tRNA-derived small RNAs. *Cell* **170**, 61–71 (2017).
23. Teunissen, S. W. et al. Conserved features of Y RNAs: a comparison of experimentally derived secondary structures. *Nucleic Acids Res.* **28**, 610–619 (2000).
24. Lerner, M. R., Boyle, J. A., Hardin, J. A. & Steitz, J. A. Two novel classes of small ribonucleoproteins detected by antibodies associated with lupus erythematosus. *Science* **211**, 400–402 (1981).
25. Weibrecht, I. et al. In situ detection of individual mRNA molecules and protein complexes or post-translational modifications using padlock probes combined with the in situ proximity ligation assay. *Nat. Protoc.* **8**, 355–372 (2013).
26. Ma, Y. et al. Spatial imaging of glycoRNA in single cells with ARPLA. *Nat. Biotechnol.* **42**, 608–616 (2024).
27. Liu, H. et al. In situ visualization of RNA-specific sialylation on living cell membranes to explore N-Glycosylation sites. *J. Am. Chem. Soc.* **146**, 8780–8786 (2024).
28. Li, J. et al. Novel approach to enriching glycosylated RNAs: specific capture of glycoRNAs via solid-phase chemistry. *Anal. Chem.* **95**, 11969–11977 (2023).
29. Xie, Y. et al. The modified RNA base acp3U is an attachment site for N-glycans in glycoRNA. *Cell* **187**, 5228–5237 (2024).
30. Zhang, N. et al. Cell surface RNAs control neutrophil recruitment. *Cell* **187**, 846–860 (2024).
31. Perr, J. et al. RNA-binding proteins and glycoRNAs form domains on the cell surface for cell-penetrating peptide entry. *Cell* **188**, 1878–1895 (2025).
32. Sharma, S., Jiao, X., Yang, J., Kwan, K. Y. & Kiledjian, M. Extracellular exosomal RNAs are glyco-modified. *Nat. Cell Biol.* **27**, 983–991 (2025).
33. Ren, T. et al. FRET imaging of glycoRNA on small extracellular vesicles enabling sensitive cancer diagnostics. *Nat. Commun.* **16**, 3391 (2025).
34. Saxon, E. & Bertozzi, C. R. Cell surface engineering by a modified Staudinger reaction. *Science* **287**, 2007–2010 (2000).
35. Debets, M. F. et al. Metabolic precision labeling enables selective probing of O-linked N-acetylgalactosamine glycosylation. *Proc. Natl. Acad. Sci. USA* **117**, 25293–25301 (2020).
36. Ohn, T., Kedersha, N., Hickman, T., Tisdale, S. & Anderson, P. A functional RNAi screen links O-GlcNAc modification of ribosomal proteins to stress granule and processing body assembly. *Nat. Cell Biol.* **10**, 1224–1231 (2008).
37. Dhir, A. et al. Mitochondrial double-stranded RNA triggers antiviral signalling in humans. *Nature* **560**, 238–242 (2018).
38. James, L. R. et al. Flux through the hexosamine pathway is a determinant of nuclear factor κB-dependent promoter activation. *Diabetes* **51**, 1146–1156 (2002).
39. Kronlage, M. et al. O-GlcNAcylation of histone deacetylase 4 protects the diabetic heart from failure. *Circulation* **140**, 580–594 (2019).
40. Bose, T. et al. Origin of life: protoribosome forms peptide bonds and links RNA and protein dominated worlds. *Nucleic Acids Res.* **50**, 1815–1828 (2022).
41. Chen, M. C. et al. Structural basis of G-quadruplex unfolding by the DEAH/RHA helicase DHX36. *Nature* **558**, 465–469 (2018).
42. Mamot, A. et al. Ethylenediamine derivatives efficiently react with oxidized RNA 3′ ends providing access to mono and dually labelled RNA probes for enzymatic assays and in vivo translation. *Nucleic Acids Res.* **50**, e3 (2022).
43. Li, A. Y. Z. et al. Milton assembles large mitochondrial clusters, mitoballs, to sustain spermatogenesis. *Proc. Natl. Acad. Sci. USA* **120**, e2306073120 (2023).
44. Danylchuk, D. I., Jouard, P. H. & Klymchenko, A. S. Targeted solvatochromic fluorescent probes for imaging lipid order in organelles under oxidative and mechanical stress. *J. Am. Chem. Soc.* **143**, 912–924 (2021).
45. Degen, W. G. J., Pruijn, G. J. M., Raats, J. M. H. & van Venrooij, W. J. Caspase-dependent cleavage of nucleic acids. *Cell Death Differ* **7**, 616–627 (2000).
46. Li, Z. et al. TIPE3 is a candidate prognostic biomarker promoting tumor progression via elevating RAC1 in pancreatic cancer. *Mol. Cancer* **21**, 160 (2022).
47. Qin, W. et al. Artificial cysteine S-glycosylation induced by per-O-acetylated unnatural monosaccharides during metabolic glycan labeling. *Angew. Chem. Int. Ed.* **57**, 1817–1820 (2018).
48. Bergeron-Brlek, M. et al. A convenient approach to stereoisomeric iminocyclitols: generation of potent brain-permeable OGA inhibitors. *Angew. Chem. Int. Ed.* **54**, 15429–15433 (2015).
49. Whitworth, G. E. et al. Analysis of PUGNAc and NAG-thiazoline as transition state analogues for human O-GlcNAcase: mechanistic and structural insights into inhibitor selectivity and transition state poise. *J. Am. Chem. Soc.* **129**, 635–644 (2007).
50. Chou, T. Y., Dang, C. V. & Hart, G. W. Glycosylation of the C-Myc transactivation Domain. *Proc. Natl. Acad. Sci. USA* **92**, 4417–4421 (1995).
51. Li, C. et al. Selective sorting and secretion of hY4 RNA fragments into extracellular vesicles mediated by methylated YBX1 to promote lung cancer progression. *J. Exp. Clin. Canc. Res.* **41**, 136 (2022).
52. van Zonneveld, A. J., Zhao, Q., Rotmans, J. I. & Bijkerk, R. Circulating non-coding RNAs in chronic kidney disease and its complications. *Nat. Rev. Nephrol.* **19**, 573–586 (2023).

53. Joyner, J. C., Keuper, K. D. & Cowan, J. A. Analysis of RNA cleavage by MALDI-TOF mass spectrometry. *Nucleic Acids Res.* **41**, e2 (2013).
54. Lee, J. H. et al. Restriction fragment mass polymorphism (RFMP) analysis based on MALDI-TOF mass spectrometry for detecting antiretroviral resistance in HIV-1 infected patients. *Clin. Microbiol. Infec.* **19**, E263–E270 (2013).
55. Carré, C. et al. tRNA 2′-O-methylation by a duo of TRM7/FTSJ1 proteins modulates small RNA silencing in Drosophila. *Nucleic Acids Res.* **48**, 2050–2072 (2020).
56. Laughlin, S. T. et al. Metabolic labeling of glycans with azido sugars for visualization and glycoproteomics. *Methods Enzymol* **415**, 230–250 (2006).
57. Hartmer, R. et al. RNase T1 mediated base-specific cleavage and MALDI-TOF MS for high-throughput comparative sequence analysis. *Nucleic Acids Res.* **31**, e47 (2003).
58. Lou, X. et al. Fragmentation of organic ions bearing fixed multiple charges observed in MALDI MS. *J. Mass. Spectrom.* **53**, 39–47 (2018).
59. Cheng, H. et al. Chemical deprenylation of N6-Isopentenyladenosine (i6A) RNA. *Angew. Chem. Int. Ed.* **59**, 10645–10650 (2020).
60. Ren, X. et al. Single-cell imaging of m^6A modified RNA using m^6A-specific in situ hybridization mediated proximity ligation assay (m^6AISH-PLA). *Angew. Chem. Int. Ed.* **60**, 22646–22651 (2021).
61. Fredriksson, S. et al. Protein detection using proximity-dependent DNA ligation assays. *Nat. Biotechnol.* **20**, 473–477 (2002).
62. Zhang, K. et al. Direct visualization of single-nucleotide variation in mtDNA using a CRISPR/Cas9-mediated proximity ligation assay. *J. Am. Chem. Soc.* **140**, 11293–11301 (2018).
63. Deng, R. et al. DNA-sequence-encoded rolling circle amplicon for single-cell RNA imaging. *Chem* **4**, 1373–1386 (2018).
64. Ke, R. et al. Improving precision of proximity ligation assay by amplified single molecule detection. *PLoS ONE* **8**, e69813 (2013).
65. Kaushik, S. & Cuervo, A. M. Chaperone-mediated autophagy: a unique way to enter the lysosome world. *Trends Cell Biol* **22**, 407–417 (2012).
66. Yang, Y. et al. OGT suppresses S6K1-mediated macrophage inflammation and metabolic disturbance. *Proc. Natl. Acad. Sci. USA* **117**, 16616–16625 (2020).
67. Rodrigo, F. et al. A small molecule that inhibits OGT activity in cells. *ACS Chem. Biol.* **10**, 1392–1397 (2015).
68. Barkovskaya, A. et al. O-GlcNAc transferase inhibition differentially affects breast cancer subtypes. *Sci. Rep.* **9**, 5670 (2019).

Acknowledgements

We gratefully acknowledge the National Natural Science Foundation of China (22474057 granted to Y.C.).

Author contributions

All authors contributed to this work. Y.R., Y.M., H.L., G.L. and J.S. performed biochemical, cellular, confocal fluorescence imaging, gel electrophoresis and mass spectrometric analyses. All authors discussed the results. L.D., Y.C. and H.J. checked the background in glycobiology. Y.R., Y.C. and H.J. wrote the manuscript. Y.R. and Y.C. designed the studies. Y.C. and H.J. supervised the project.

Competing interests

The authors declare no competing interests.

Additional information

Supplementary information The online version contains supplementary material available at https://doi.org/10.1038/s41467-026-72909-4.

Correspondence and requests for materials should be addressed to Yunlong Chen or Huangxian Ju.

Peer review information *Nature Communications* thanks the anonymous reviewers for their contribution to the peer review of this work. A peer review file is available.